SEMMELWEIS EGYETEM

DOKTORI ISKOLA

**Ph.D. értekezések**

**XXXX.**

**VAJDA FLÓRA**

Molekuláris Orvostudományi Tagozat

Patobiokémia Program

Programvezető: Dr. Várnai Péter, egyetemi tanár

Témavezető: Dr. Szakács Gergely, tudományos főmunkatárs

Társtémavezető: Dr. Füredi András, tudományos munkatárs

# INVESTIGATING THE ROLE OF MESENCHYMAL STEM CELLS IN CANCER DRUG RESISTANCE

**PhD thesis**


## Flóra Vajda

Semmelweis University Doctoral School

Molecular Medicine Division


| | |
|---|---|
| Supervisor: | Gergely Szakács, MD, Ph.D. |
| Co-supervisor: | András Füredi, Ph.D. |
| Official reviewers: | Judit Kiss, Ph.D.<br>Lőrinc Pongor, Ph.D. |

Head of the Complex Examination Committee: Sára Tóth, habil. Ph.D.

Members of the Complex Examination Committee: Veronika Urbán, Ph.D.
Matula Zsolt, Ph.D.

Budapest
2024

## Table of Contents

## List of Abbreviations

2D - 2 dimension

3D - 3 dimension

α-SMA - alpha-smooth muscle actin

ABC - ATP-binding cassette

Ad-MSC - adipose-derived mesenchymal stem cell

ATM - ataxia-telangiectasia mutated

Bcl-2 - B-cell lymphoma 2

BDNF - brain-derived neurotrophic factor

bFGF - basic fibroblast growth factor

BM - bone marrow

BMP - bone morphogenetic protein

BRCA1, BRCA2 - breast cancer 1 and 2 protein

CAF, TAF - cancer-associated fibroblast, tumor-associated fibroblast

CAR - chimera antigene receptor

CCL5 - C-C Motif Chemokine Ligand 5

$CoCl_2$ - cobalt chloride

CTL - cytotoxic T lymphocytes

CYP-enzyme - cytochrome P450 enzyme

DCFH-DA - 2'-7' dichlorofluorescein diacetate

DCH - 2′,7′-dichlorofluorescein

DHFR - dihydrofolate reductase

DNA - deoxyribonucleic acid

DSB - double-strand break

EF1 - elongation factor-1

EGFR - epidermal growth factor receptor

FACS – fluorescence-activated cell sorting

FAP - fibroblast activation protein

FBS - fetal bovine serum

FDA - Food and Drug Administration

FGF-2 - fibroblast growth factor 2

FSP-1 - ferroptosis suppressor protein 1

GFP - green fluorescent protein

GM-CSF - granulocyte-macrophage colony-stimulating factor

$H_2O_2$ - hydrogen-peroxide

HFF - human foreskin fibroblast

HGF - hepatocyte growth factor

HIF1-α – hypoxia-inducible factor 1-alpha

$IC_{50}$ – half-maximal inhibitory concentration

iDNMTS - DNA methyltransferase inhibitors

IFN-γ - interferon gamma

IGF-1 - insulin-like growth factor 1

IGF-2 - insulin-like growth factor 2

IGFBP-2 - insulin-like growth factor binding protein 2

iHDACs - histone deacetylase inhibitors

IDO - Indoleamine 2,3-dioxygenase

IL-1β - interleukin-1 beta

IL-6 - interleukin-6

IL-8 - interleukin-8

IRAK4 - interleukin-1 receptor-associated kinase 4

ISCT - International Society for Cellular Therapy

LIF - leukaemia inhibitory factor

mCh - mCherry fluorescent protein

M-CSF - macrophage colony-stimulating factor

MDM2 - mouse double minute 2

MIF - macrophage inhibitory factor

MIP-2 - macrophage inflammatory protein-2

MMPs - matrix metalloproteinases

MSC - mesenchymal stem cell

NF-kB - nuclear factor kappa-light-chain-enhancer of activated B cells

PBS - phosphate buffer saline

PARP-1 - poly-ADP ribose polymerase-1

PD-1/PD-L1 - programmed cell ceath protein 1, programmed death-ligand 1

PDGF - platelet-derived growth factor

PDGFr-α - platelet-derived growth factor receptor alpha

PFA - paraformaldehyde

PGE2 - prostaglandin E2

PGP - P-glycoprotein

PI3Ks - phosphoinositide 3-kinases

PTEN - phosphatase and tensin homolog

RNA - ribonucleic acid

ROS - reactive oxygen species

S1PR1 - sphingosine-1-phosphate receptor-1

SA-ß-gal - senescence-associated beta-galactosidase

SDF-1α - stromal cell-derived factor 1

TGF-β - transforming growth factor-β

TIS - treatment induced senescence

TME - tumor microenvironment

TNF-α - tumor necrosis factor alpha

TRAIL - TNF-related apoptosis-inducing ligand

TSP-1 - thrombospondin 1

VEGF - vascular endothelial growth factor

# 1. Introduction

## 1.1. Prevalence of Cancer

According to incidence and mortality data from the Global Cancer Observatory, 20 million people are diagnosed with cancer, and 10 million die from various types of tumors each year (1). Sixty percent of patients diagnosed with cancer are treated with conventional or novel (targeted or immuno) chemotherapies, but the response is highly dependent on genetic and individual characteristics. Initially, malignancies respond well to treatment, but over time, drug resistance emerges, and cancer cells become less sensitive to drugs, even to compounds that have not been used before (2). After successive cycles of chemotherapy, tumor cells evade apoptosis and develop a more aggressive phenotype that is more difficult to cure.

## 1.2. Possible mechanisms of drug resistance in cancer cells

The modern era of cancer treatment started in the 1940s when cytotoxic and cytostatic agents were developed (3). Since then, drug resistance has remained one of the major challenges (4). After remission, the tumor often reappears with altered molecular and genetic characteristics, rendering it insensitive to compounds previously applied and also to other compounds that have never been used before to treat the patient (5).

Combating cancer is one of the greatest challenges in modern medicine, as malignant cells are extremely persistent and can adapt to virtually any environment or insult. Drug-resistant cancer cells can efflux drug molecules (6) or enzymatically inactivate different chemotherapeutics (7), mobilize different DNA repair proteins (8), avoid apoptosis by distorting apoptotic pathways (9), reduce the expression of target proteins (10) or temporarily suspend cell cycle to evade compounds that kill rapidly dividing cells (11) (Fig. 1.). In addition, recent discoveries have further expanded the known mechanisms of resistance: damage to the tumor microenvironment (TME) can promote resistance to cancer drugs (12) and treatment-induced epigenetic changes can result in drug-tolerant persister cells (13). Tumor heterogeneity, the presence of different cell populations with diverse molecular characteristics and drug sensitivity in the tumor also fuels resistance (14), as does the evasion of immunosurveillance (15).

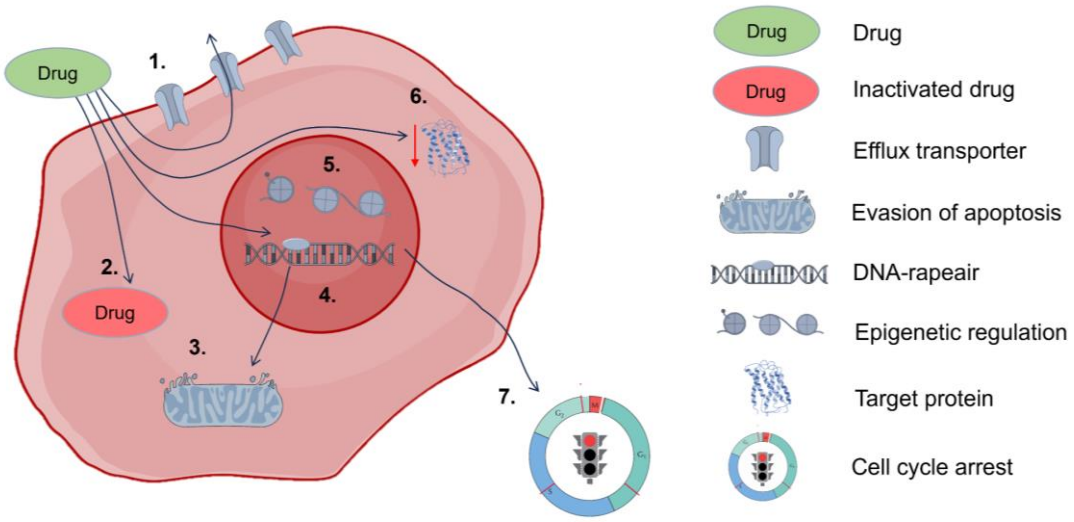


***Figure 1.*** *Cellular mechanisms of drug resistance. Active efflux transporters (1) or inactivation of drug molecules (2), altered response to apoptotic signals (3), increased DNA repair activity (4), epigenetic gene regulation (5), reduction in target protein expression (6) and exit from cell cycle (7) (16).*

One way cancer cells become resistant by overexpressing transmembrane efflux pumps to expel cytotoxic and cytostatic agents. Elevated levels of ATP-binding cassette (ABC) transporters are responsible for multidrug resistance; they actively pump certain drugs out of the cell, reducing the effectiveness of chemotherapy (17) (Fig. 1. (1)). Increased PGP expression was detected in glioblastoma cells following doxorubicin treatment, resulting in continuous release of the molecule (18).

The human CYP-family is mostly expressed in hepatocytes, but also kidney, lung and tumor cells express CYP-enzymes responsible for drug inactivation or biotransformation. This altered drug metabolism involves the detoxification of chemotherapeutic agents through metabolic pathways regulated by the high expression of cytochrome P450 enzymes (19) (Fig. 1. (2)). Cytochrome P450 3A4, one of the major members of the CYP-family, reduces the bioavailability of paclitaxel by converting it to 3′-p-hydroxypaclitaxel and 6a, 3′-p-dihydroxypaclitaxel (20).

Alterations in apoptotic pathways, with the expression of certain mitochondrial proteins, allow tumor cells to escape apoptosis. For example, in chronic myeloid leukemia

following imatinib treatment, tumor cells were observed to increase Bcl-2 antiapoptotic protein levels, which inhibited apoptosis (21) (Fig. 1. (3)).

Most anti-tumor agents induce programed cell death or necrosis in tumor cells by causing significant DNA damage. Tumor cells overexpress DNA-repair proteins (ATM, BRCA1, BRCA2, RAD51 and PARP1) for more efficient genetic repair, resulting in cancer cell survival despite extensive DNA-damage (22) (Fig. 1. (4)).

Epigenetic alterations such as changes in DNA methylation, histone modifications, chromatin remodeling, and expression of non-coding RNAs can permanently affect drug sensitivity by switching on and off resistant genes and by regulating DNA accessibility of drugs via modifying chromatin structure. Drugs that erase these epigenetic patterns (DNA methyltransferase inhibitors (iDNMTs) and histone deacetylase inhibitors (iHDACs)) may restore sensitivity to chemotherapy in patients (5) (Fig.1. (5)).

Tumor cells downregulate the expression of proteins specifically targeted by chemotherapeutic agents. The expression of DNA-synthesis proteins, such as topoisomerase I and II, is reduced following doxorubicin treatment, eliminating target protein expression. This provides protection against topoisomerase-targeting drugs (23) (Fig. 1. (6)).

Cell cycle inhibitors (paclitaxel, vinblastine) target only at a certain phase of the cell cycle, so their use against cancer cells at different stages of the cell cycle is limited. To combat this kind of drug resistance, they are often used as part of combination therapies. For example, paclitaxel inhibits the tubulin-assembly cell cycle specifically from metaphase to anaphase (24).

### 1.3. Tumor microenvironment and drug resistance

A new therapeutic approach has emerged with definition of the TME as a complex ecosystem that includes not only cancer cells but also immune cells, mesenchymal stem cells (MSC)/fibroblasts, blood vessel-forming endothelial cells and cancer stem cells (Fig. 2.). Non-cellular components include extracellular matrix components, such as laminin, fibronectin and collagen fibres, secreted cytokines and chemokines and

microvesicles or exosomes. This extends the focus beyond the targeted destruction of tumor cells.

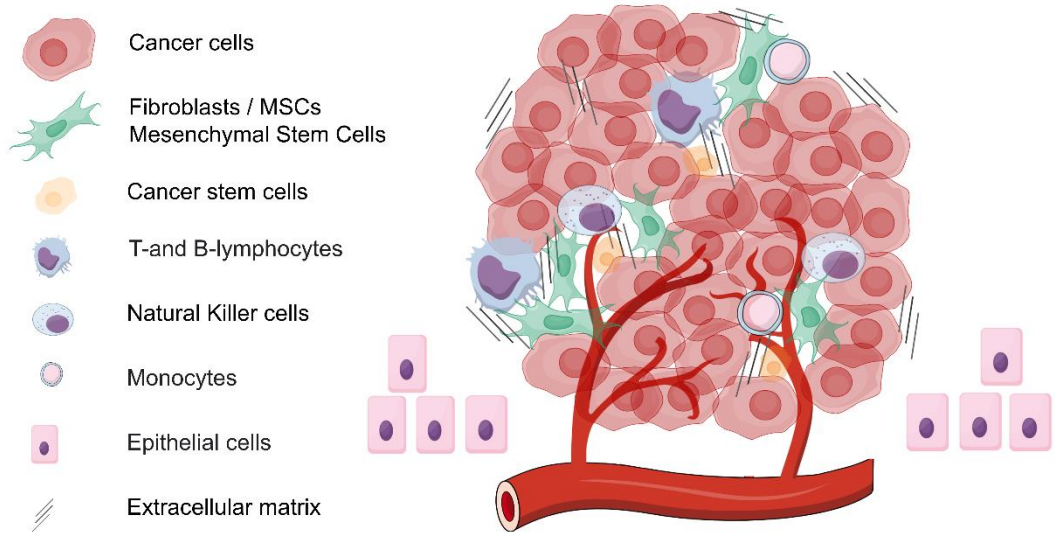


***Figure 2.*** *Tumor stroma is a complex heterogeneous network of cells including cancer cells, mesenchymal stem cells (MSCs)/fibroblasts, immune cells, cancer stem cells and vascular endothelial cells embedded into extracellular matrix.*

Treatments that directly kill tumor cells include alkylating agents, plant alkaloids, antimetabolites, anthracyclines, topoisomerase inhibitors and corticosteroids, whereas indirect treatment strategies such as anti-angiogenic therapies, immunotherapies, hypoxia or acidosis inhibition, aims to degrade the extracellular matrix and microvesicles/exosomes or exosomes (25, 26).

Anti-vascular therapies (bevacizumab, sunitinib and pazopanib) stop the formation of new blood vessels (27), which disrupts nutrients and oxygen supply by reducing vascularization. This leads to tumor cell deprivation. This can lead to cellular stress, metabolic alterations and cancer cell death. Resistance to anti-VEGF therapies activates different angiogenic pathways in cancer, such as Angiopoetin-Tie or FGF-FGFR signaling (28).

The immune response can probably be boosted by using targeted monoclonal antibodies that recognize specific proteins on cancer cell membranes. This tumor antigen and antibody barrier is recognized by the immune system, and this signal helps T-cells and

NK-cells to clear cancerous cells. In solid tumors, anti-EGFR (mAb335, cetuximab and panitumumab) or anti-PD1/PD-L1 antibodies (nivolumab, toripalimab) recognize specific tumor antigens and activate the immune response (29, 30). Another novel type of immunotherapy is chimera antigen receptor (CAR) T-cell therapy. In CAR T-cell therapy, T-cells are extracted from patient blood and reprogramed with CAR gene by lentiviral transfection. Engineered T-cells are expanded and infused back to the patient, which can attach to specific tumor antigens, killing tumor cells. CAR T-cell therapy is used after other types of treatment that have proved to be ineffective (31). The role of cytotoxic CD8+ T cells (CTLs) in therapy resistance is clearly demonstrated by the strong correlation between the CTL profile of tumors and their response to neoadjuvant therapy. Breast tumors with strong lymphocyte infiltration had a pathological complete response of more than 40% after taxane treatment, whereas only 7% of tumors without any detectable lymphocyte population showed a similar response, suggesting that the CTL profile is an independent prognostic factor (32).

In solid tumors, the pH decreases to 6.8 compared to normal tissue, where the pH is 7.2. Increased anaerobic glycolysis and lactate production lead to an acidic, or rather, rapid proliferation of cancer cells, fenestrated blood vessels and poor oxygen supply create a hypoxic environment (33-35). Hypoxia and acidosis inhibition strongly affect vascularization and cancer cell metabolism through HIF-1α related signaling pathways. HIF-1α plays a role in the adaptation to low oxygen level and upregulation of erythropoietin, VEGF, and glucose transporters (36). Consequently, altered metabolic pathways, such as switching to anaerobic glycolysis promote cancer cell survival (37).

MMPs enzymes degrade the fibrous structure of TME. MMP inhibitors prevent the rupture of connective tissues surrounding the tumor region, inhibit tumor cell invasion and metastasis as physical barriers. Although the therapy initially appeared to be promising, it did not live up to expectations, as these agents failed to selectively break down the extracellular matrix. As a result, they did not receive FDA approval (38).

Communication between tumor cells and non-malignant stromal cells which constitute TME is crucial in the pathophysiology of cancer. MSCs are versatile stromal stem cells that are present in most cancers and play a pivotal role in TME development and function.

MSCs have been shown to promote tumor growth through various mechanisms, but conversely, MSCs have also been reported to exhibit anti-tumorigenic properties.

MSCs are mostly located in adipose tissues and bone marrow, but the appearance of tumor cells can attract MSCs to create a supportive environment (39). This is a possible way for tumors to create their own microenvironment, incite MSCs to exit their naive state, and enter into a primed condition as CA-MSCs/CAFs, expressing specific markers (40).

MSCs are known to play a dual role in tumor development: both tumor-promoting and tumor-inhibiting effects have been described in the literature. MSCs can mostly influence their environment through secreted factors such as VEGF, FGF-2, PDGF, HGH, BDNF, SDF-1α, IGF-1, IGF-2, TGF-β, TNF-α, IGFBP-2, LIF, M-CSF, MIP-2, IL-6, IL-8 and IFN-γ cytokines, which canincrease cancer cell proliferation and survival even after chemotherapeutictreatment. IL-6, bFGF and PGE2 are types of chemokines that accelerate tumor cell growth (41). VEGF strongly influences vascularization by promoting angiogenesis, thus supplying tumor cells with essential nutrients and oxygen (41). However, the effect of MSCs has also been described as pro-angiogenic and anti-angiogenic (by secretion of TSP-1 and endostatin). In addition, the presence of MSCs increase c-myc, wnt expression and modify PI3K/AKT, and JAK2/STAT3 signaling pathways, which promote proliferation even after drug treatment (42, 43). S1PR1 expression is also induced in tumors by human bone-marrow MSCs, which makes the tumors resistant to chemotherapy (44). The anti-inflammatory effect of MSCs is primarily mediated by the secretion of regulatory T-cell mediated cytokines PGE2 and IDO. In additione, the cytotoxic cytokine TRAIL induces axis-related apoptotic pathways TNF-α-TRAIL in glioblastoma cells (45). Similarly, anti-proliferative factors released by MSCs, such as BMP and PTEN, also influence tumor progression. MSCs produce interferons, such as IFN-β, which have anti-proliferative and immunomodulatory effects on cancer cells. Secreted soluble factors, such as IL-10, TNF-α, and TGF-β, modulate the tumor microenvironment and suppress tumor growth and progression (41, 46).

Disrupting the supportive niche that protects cancer cells and helps them survive could significantly increase the efficacy of currently used treatment strategies. First, however, the precise role of TME in tumor biology needs to be understood.

### 1.4. From naive to primed MSCs: MSCs vs CAFs

MSCs/fibroblasts are cells that maintain the structural integrity of connective tissue and play a role in tissue repair and regeneration. Naive MSCs can be isolated from BM, adipose tissue and cord blood for research purposes. This naive state of MSCs is when they are involved in tissue homeostasis and regeneration and have not yet undergone differentiation. These MSCs remain in their multipotent and naive state and can be a potential avenue of exploring stem cell biology and regenerative medicine (47).

Primed condition appears when MSCs exit the naive state due to specific signaling cues or differentiation factors. Adipose-derived MSCs are spindle-shaped, elongated morphologically and can be easily differentiated into fat cells (adipocytes), bone cells (osteoblasts), or cartilage cells (chondrocytes) *in vitro* (48). Due to their high migratory capacity, MSCs can migrate into the tumor environment in response to chemoattractant signals released by tumor cells to establish a supportive tumor nest. During early tumor development, naive MSCs repress tumor cells, but later differentiate/transform into cancer-associated MSCs or fibroblasts (CAF) in a primed or activated condition. MSCs secrete factors with various anti-tumor properties, including cytokines, chemokines, and growth factors, which can inhibit tumor cell proliferation, induce apoptosis and suppress angiogenesis. Naive MSCs secrete PGE2, lactate and TGF-β, which inhibit tumor growth. Cytokines CCL5, IFN-γ and TGF-β promote EMT, so epithelial cancer cells can increase invasion and metastasis by acquiring mesenchymal features (49, 50). Elevated expression of cyclin A, cyclin D2 and cyclin E in response to MSC cytokines freezes tumor cells in $G_1$ phase (51). In addition to studies on the effects of conditioned media, co-cultural experiments have also confirmed similar phenomena (52). MSCs can remodel the extracellular matrix and alter the physical properties of the tumor stroma. This remodelling can create a less permissive microenvironment for tumor growth and invasion, making it more difficult for cancer cells to proliferate and metastasize.

Tumor cells strongly influence the behaviour of the surrounding cells, while conditioned MSCs acquire a new phenotypic and genotypic appearance. This leads to CAF becoming an active stromal compartment in the TME. Inhibition of the Hedgehog pathway and immunotherapy against the FGFR and TGF-β attenuate the tumor-supporting effect of CAFs. However, the confirmation of the therapeutic effect of these compounds is still

only in clinical phases I and II (53, 54). Through HGF secretion, CAFs can induce drug resistance to EGFR inhibitors in colon cancer cells by activating the MET pathway (55). Similarly, WNT16B expression following chemotherapeutic treatment is also increased in CAF cells, which leads to NF-κB activation of surrounding prostate cancer cells, ultimately inducing resistance (12). In pancreatic cancer cells and tumors, IL-1β secretion and IRAK4 co-expression in CAFs also lead to gemcitabine resistance via the NF-κB pathway, to the extent that the inhibition of IRAK4 restores gemcitabine sensitivity (56). It has been observed in human hepatocarcinoma that isolated CAF cells stimulated EMT in liver carcinoma cells by producing IL-6 and HGF cytokines. Increased expression of TG-2 was mediated through the IL-6 cytokine and STAT3 pathway, which promoted tumor cell EMT (57).

These activated CAF cells express specific markers that can be used to identify them: α-SMA, PDGFr-α and (CD140a and b), FSP-1 and FAP (58). Therefore, new cellular characterization studies are essential to standardize the identification of CAF cells in order to understand different interactions between CAF cells and cancer cells. CAFs constitute the largest part of the tumor stroma (50-90%) and may be promising therapeutic targets for cancer treatment (59).

Understanding the controversial role of MSCs in TME is a challenging but important task. It would certainly be beneficial to develop treatment strategies targeting CAF that may supplement conventional chemotherapy or even modern targeted/immunotherapies. However, the lack of basic understanding of the interactions between appropriate *in vitro* models and MSC-cancer cell is a major impediment to this effort. This research proposal intends to investigate the effects of chemotherapy on both MSCs and cancer cells, establish co-culture models for drug testing and study the interaction between the two cell types.

# 2. Objectives

In my PhD research, I set the following objectives:

➤ to investigate the response of human MSCs and tumor cells to different chemotherapeutic treatments, individually and separately, and in co-cultures

➤ to compare the toxicity of nine different compounds (namely bendamustine, cisplatin, doxorubicin, irinotecan, methotrexate, mitoxantrone, nutlin-3, TPEN and vinblastine) with different structures and mechanisms of action in different types of MSCs (Ad-MSC-GFP 1,2,3, BM-MSC and HFF) and cancer cells (MCF-7-GFP, MES-SA-mCherry and A431-mCh)

➤ to investigate the response of MSCs and cancer cells to chemotherapy: DNA double-stranded breaks, induction of reactive oxygen species (ROS), senescence and apoptosis

➤ to establish and characterize 2D monolayer and 3D spheroid co-cultures using MSCs and cancer cells to model TME

➤ to test and compare drug sensitivity of 2D vs. 3D MSCs and cancer cell co-cultures

# 3. Methods

## 3.1. Establishment and characterization of a new BM-MSC cell line

BM-cell line was established from a 4-year-old female pediatric patient. BM-MSC was obtained by BM-biopsy and characterized *in vitro* according to the International Society for Cellular Therapy guidelines (ISCT). The novel cell line was evaluated based on the fundamental criteria required for establishing a new MSC line, including adherence to plastic, expression of specific CD markers, and ability to undergo differentiation. The research was approved by the Ethical Committee of the Hungarian Medical Research Council (ETT; ID: 24083-3/2013/HER).

## 3.2. Cell lines

The Adipose-derived Mesenchymal Stem Cell 1 (Ad-MSC 1) cell line was established from adipose tissue obtained via lipoaspiration from the femoral region of a 30-year-old female. Ad-MSC 2 and 3 cell lines were obtained from a surgical sample from the haunch area of a 5-year-old female, and a 4-year-old male donor. Cell lines were established by Creative Cell Ltd. in 2005. HFF, MES-SA, MCF-7 and A431 cell lines were purchased from ATCC (Table 1).

***Table 1.*** *Summary table on the background of cells.*

| Human cell lines | Cell type | Age | Sex | Source |
|---|---|---|---|---|
| Ad-MSC 1 | Adipose derived mesenchymal stem cell | 30 | Female | Creative Cell Ltd. |
| Ad-MSC 2 | Adipose derived mesenchymal stem cell | 5 | Female | Creative Cell Ltd. |
| Ad-MSC 3 | Adipose derived mesenchymal stem cell | 4 | Male | Creative Cell Ltd. |
| BM-MSC | Bone-marrow mesenchymal stem cell | 4 | Female | Creative Cell Ltd. |
| HFF | Human foreskin fibroblast | 1 | Male | ATCC |
| MCF-7 | Breast epithelial adenocarcinoma | 69 | Female | ATCC |
| MES-SA | Uterine sarcoma | 56 | Female | ATCC |
| A431 | Skin squamous cell carcinoma | 87 | Female | ATCC |

### 3.3. Cell culturing

In our comparative experiments, we used a panel of six MSC-like cells and three cancer cell lines. Three human primary adipose tissue-derived MSCs, namely Ad-MSC 1,2,3, one BM-MSC and one HFF (ATCC) cell line underwent drug screening. MCF-7, MES-SA and A431 (ATCC) cell lines were used to represent cancer cells. All cell lines were cultured in supplemented DMEM-12 to avoid alterations in results due to different culture conditions. The basal culture medium was complemented with 10% FBS, 1% L-glutamine, 0,1% gentamicin, and 0,16 ng/ml fibroblast growth factor 2.

### 3.4. GFP and mCherry transduction

After lipoaspiration from human donors, the tumescent tissue was digested with 0.1% w/v% collagenase (Sigma) and plastic adherent Ad-MSCs were plated in cell culture media. Lentiviral vectors expressing eGFP or mCherry genes under the regulation of human EF1 promoter flanked by LTR sequences were generated using a second-generation packaging system for self-inactivating lentiviral vectors. The titer was determined by transduction of HEK293 cells followed by flow cytometry. When the percentage of infected cells is below 20%, the number of integrations is approximately equal to the number of transduced cells. Thus, the number of infectious virus particles per given volume can be determined as Transduction Units per ml (TU/ml). GFP-positive cells were sorted after transduction using a FACS Aria I flow cytometer. The same protocol was used to establish the A431-mCherry subline.

### 3.5. Cytotoxicity assay

Cells were plated in a 96-well tissue culture plate in 100µl DMEM-12 media. MSCs/fibroblast cells were seeded at a concentration of $5x10^3$/100µl/well and cancer cells at a density of $4x10^3$/100µl/well. For spheroid formation assay, $1x10^4$ cells were plated in a U bottom plate with a cell-repellent surface. Cells were allowed to attach or aggregate overnight and then treated with serially diluted concentrations of bendamustine, cisplatin, doxorubicin, irinotecan, methotrexate, mitoxantrone, nutlin-3, TPEN and vinblastine in 100µl DMEM-F12 the following day. The mechanism of action and source of compounds are listed in Table 2. PrestoBlue™ Cell Viability Reagent (Thermo) was used to determine cell viability (0-100%). Due to metabolic differences,

cells were incubated with diluted 5-12.5% PrestoBlue solution in PBS (MSCs: 12.5%, Cancer cells: 5%). The fluorescence of PrestoBlue reagent was measured with an EnSpire fluorometer at 555nm (ex) / 585nm (em) wavelength. Data were normalized to the fluorescence of blank sample (media) and sigmoidal dose-response curves were fitted using logarithm and least square method.

***Table 2.*** *List of compounds used in cytotoxicity assay.*

| Compounds | Mechanism of action | Source |
|---|---|---|
| Bendamustine | DNA intrastrand crosslinker | Servier |
| Cisplatin | DNA interstrand crosslinker | Accord Healthcare |
| Irinotecan | Topoisomerase I inhibitor | abcr |
| Doxorubicin | Topoisomerase II inhibitor | Sigma Aldrich |
| Mitoxantrone | Topoisomerase II inhibitor | Sigma Aldrich |
| Methotrexate | Purine and pyrimidine biosynthesis inhibitor | Sigma Aldrich |
| Nutlin-3 | p53 stabilisation, MDM2 inhibitor | Tocris |
| TPEN | ROS generator and metal chelator | Tocris |
| Vinblastine | Tubulin synthesis inhibitor | MedChemExpress |

### 3.6. Cell Proliferation assay

The fluorescent CytoTell™ Green dye (AAT Bioquest) was used to analyze differences in cell proliferation rate. Cells were centrifuged and $3x10^5$ cells were stained with 2µl CytoTell™ dye diluted in 1ml of serum-free media. Cells were incubated at 37°C for 30 min. and samples were divided into two parts. Half of the stained cells were centrifuged, plated in DMEM-F12 and analyzed on day 5, while the other part was immediately measured using Attune Nxt™ flow cytometer for baseline (day 0). Zombie Violet Dye (biolegend) was used for gating dead cells.

### 3.7. Immunohistochemistry and image analysis

Immunofluorescence staining against γ-H2AX (MA1-2022, Invitrogen) was performed in Ad-MSC-GFP 3 and A431-mCh cells with three drugs (cisplatin, doxorubicin and nutlin-3). Ad-MSC-GFP 3 cells were seeded at a concentration of $1x10^4$ and A431-mCh at $1.6x10^4$. The next day, cells were treated with 2µM cisplatin, 0.1µM doxorubicin and 30µM of nutlin-3 solution diluted in 200µl DMEM-F12. On day 5, cells were fixed with 4% PFA for 15min and washed twice with PBS. We added 100µl blocking solution

(0.5% BSA-PBS, 0.1% Triton-X, 5% goat-serum, and 1% fish gelatine) for 1h. γ-H2AX primary antibody was used at a dilution of 1:500 in blocking solution, and stained overnight at 4°C. The following day, 100µl A633-secondary antibody was added and incubated for 1h. Hoechst-33342 as a nuclei dye was diluted in PBS in 1:1000 dilution range. After fixation and blocking of cell cultures, Phalloidin-633 was diluted in a ratio of 1:1000 and used for staining with F-actin filaments. Cells were recorded using a ZEISS LSM-710 confocal microscopy at 40-fold magnification.

A semi-automated image analysis pipeline was implemented in CellProfiler™ to quantify DNA damage through γ-H2AX immunofluorescence. The process involved intensity normalization and Gaussian filtering, followed by threshold-based segmentation of DAPI-stained nucleus images to identify nuclei candidates. False candidates were manually removed, and pixel intensities were measured in the γ-H2AX channel using the remaining nuclei regions as masks to exclude non-nuclei signals.

### 3.8. Induction of reactive oxygen species (ROS)

Ad-MSC 3 and A431 cells were seeded in a 96-well tissue culture plate as described above. The cells were subsequently washed twice with HBSS and incubated in 100µL of DCFH-DA dye (R252-10, Dojindo) according to the instructions of the manufacturer. After a 30-minute incubation at 37°C, the cells were washed twice with HBSS. The cells were then treated with 200µL of cell culture medium containing appropriate concentrations of cisplatin, doxorubicin, nutlin-3 and $H_2O_2$ (as positive control) for 1 hour. The supernatant was removed, and the cells were washed with HBSS prior to imaging, using the JuLI™ Stage Cell History Recorder (NanoEntek).

### 3.9. Apoptosis assay

Apoptosis detection was based on Annexin-V molecule binding to phosphatidylserine membrane molecules. Ad-MSC 3 and A431 cells were seeded in a 12-well tissue culture plate in $5x10^4$ and $4x10^4$ cell concentration. The day after the supernatant was removed,and the cells were treated with cisplatin, doxorubicin and nutlin-3 were diluted in cell culture media at defined concentrations. After five days of treatment, we collected the supernatant, including the cells that were already dead and then the remaining attached cells were trypsinized. The cells were washed twice with 1% BSA-PBS solution

and centrifuged at 400 x g for 4 min. Next, 100µl 1x Annexin Binding Buffer was mixed with 3 µl Annexin V-Pacific Blue and 1µl TO-PRO-3 and added to each sample. The cells were incubated for 15min and diluted 5-fold with Annexin Binding Buffer and evaluated using an Attune Nxt™ flow cytometer.

### 3.10. Senescence staining

Ad-MSC 3 and A431 cells were cultured in a 96-well tissue culture plate and treated with cisplatin, doxorubicin, or nutlin-3. After 5 days, the media was removed and replaced with 200 µL of ready DMEM-F12 for a period of 7 days. Senescent cells were detected using the Senescence β-Galactosidase Staining Kit (9860S, Cell Signaling Technology). The cells were fixed with fixative solution, washed with PBS, and stained with X-gal solution overnight at 37°C without $CO_2$. Finally, the cells were coated with 70% glycerol for brightfield microscopic imaging.

### 3.11. Microscopes used for imaging

Cell growth was recorded by a JuLI™ Stage Real Time cell history recorder (NanoEntek), and an Olympus IX 51 microscope with an attached RT3 SPOT camera was used for fluorescent and brightfield imaging. Juli EDIT and Juli STAT softwares were used to analyze growth kinetics. A ZEISS LSM 710 series microscope was applied for confocal imaging.

### 3.12. Human cytokine detection

The Human Cytokine Array Kit (R&D systems, ARY005B) detects 36 different cytokines secreted by human cell lines. A total of $2x10^5$ Ad-MSC-GFP 3 cells and A431-mCh cells were seeded in a T25 tissue culture flask. For co-culture, $2x10^5$ Ad-MSC-GFP 3 cells and $2x10^5$ A431-mCh cells were seeded together. The cells were allowed to attach overnight, and the culture media was changed for a period of 3 days. This media was then replaced with 2ml serum-free DMEM-F12 to avoid detection of cytokines in FBS. On day 5, the supernatant was collected and centrifuged at 1500rpm for 5 minutes. All the reagents were prepared in advance and 2ml of Array Buffer 4 was pipetted into three chambers containing membranes. The membranes were then incubated at room temperature for 1 hour. Meanwhile, 500µl of Array Buffer 4, 200µl of Array Buffer 5,

800µl of supernatant, and 15µl of Human Cytokine Array Detection Antibody Cocktail were gently mixed and added onto the membranes for 1-hour incubation. The Array Buffer 4 mixture was aspirated from under the membranes and the sample-antibody mixture was added to the membranes. The membranes were incubated overnight at 4°C. The membranes were placed into a 50ml falcon tube and rinsed with 1X Wash Buffer on a rocking platform shaker. This washing step was repeated two more times. Streptavidin-HRP used as a positive control was diluted at a ratio of 1:2000 in Array Buffer 5. The membrane and the diluted Streptavidin-HRP solution were placed on the membrane surface, then washed and incubated for 2 minutes. The membranes were then placed in a plastic sheet container, ensuring the removal of air bubbles. The ChemiDoc™ MP (Bio-Rad) Imaging System was used to expose the membrane to X-ray for 10 minutes.

### 3.13. Establishing a 3D spheroid model and quantitative analysis of spheroid growth

$1x10^4$ Ad-MSC-GFP 3 and A431-mCh cells were seeded in 96-well 'U' bottom microplates (Corning) and allowed to self-aggregate in 100µl in DMEM-F12 with 20% FBS for 24 hours. The following day, cisplatin and nutlin-3 were diluted in cell culture media and added to the spheroids in twofold concentration. The spheroids were then examined in different compositions of Ad-MSC-GFP 3 and A431-mCh cells: 20%-80%, 50%-50%, and 80%-20%, representing different stromal ratios of tumors.

From all images containing signals from two fluorescent channels, four adjacent sites were selected for batch quantification in CellProfiler. The channel-by-channel images from the same well were combined into a single, but larger image while retaining their original intensities, and grayscale images were quantified using the intensity measurement module to obtain mean signal intensities for each combined image. The calculated mean signal intensity correlates with the observed cell confluence in the image between 0.0 and 1.0.

### 3.14. Flow cytometry analysis of 2D and 3D co-cultures

Co-culture ratios of 80% Ad-MSC-GFP 3 and 20% A431-mCh were analyzed and sorted using FACS Aria III. This ratio was chosen because otherwise tumor cells would overproliferate. Co-cultures were separated into single cell solutions with 0.2% trypsin

for 15min and 30min in 2D and 3D, respectively. Mixtures were analyzed by flow cytometry using Attune Nxt™ and TO-PRO-3 was used as a necrotic marker.

# 4. Results

## 4.1. Establishment and characterization of a novel BM-MSC

A bone-marrow mesenchymal stem cell line (BM-MSC) was established and characterized according to international standards. The cells were proved to be plastic-adherent, positive for CD44, CD73, CD90 and CD105 mesenchymal markers and negative for CD14, CD34, CD45, CD117, CD133 and HLA-DR cell surface markers (Fig. 3 A). Differentiation into osteogenic, adipogenic, and chondrogenic lineages was induced in specific cell culture media and was confirmed with Alizarin Red S, Oil Red O and 1,9-dimethyl-methylene blue (Fig. 3 B). BM-MSCs were obtained from a healthy 4-year-old female patient (Table 1).

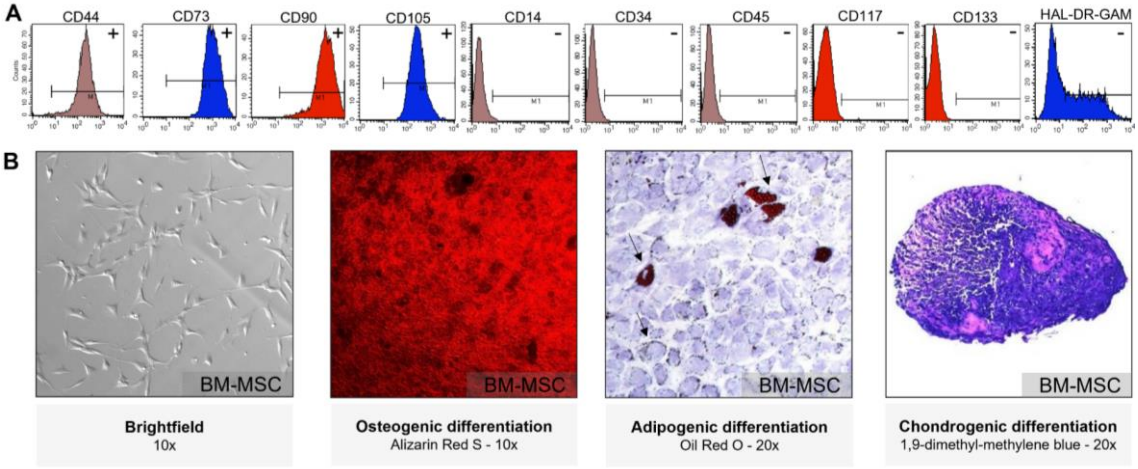


***Figure 3.*** *Characterization of a newly established BM-MSC line. Specific MSC cell surface markers were detected by flow cytometry: Positivity for CD44, CD73, CD90, CD105, negativity for CD14, CD34, CD45, CD117, CD133 and HLA-DR (A). Morphological image of BM-MSC after osteogenic, adipogenic and chondrogenic differentiation (B).*

## 4.2. Comparison of drug sensitivity of transduced and non-transduced cells

Fluorescent proteins (GFP and mCherry) were transduced with lentiviral vectors. $IC_{50}$ values and cytotoxicity curves were compared between parental cell lines (grey) and GFP (green) or mCherry (red) expressing sublines (Fig. 4 A). Viability was measured using PrestoBlue assay after cisplatin, doxorubicin and nutlin-3 treatment in three biological

parallel samples each. Dose-response curves and $IC_{50}$ values were calculated and geometric means of $IC_{50}$ values are shown in the table. (Fig. 4 B, C and D). The slopes of the curves show similarities and the $IC_{50}$ values are comparable; therefore, transduction did not affect viability and can be used for further experiments, this way fluorescence of the cells can provide additional information on the interactions between the two cells in a co-culture system.

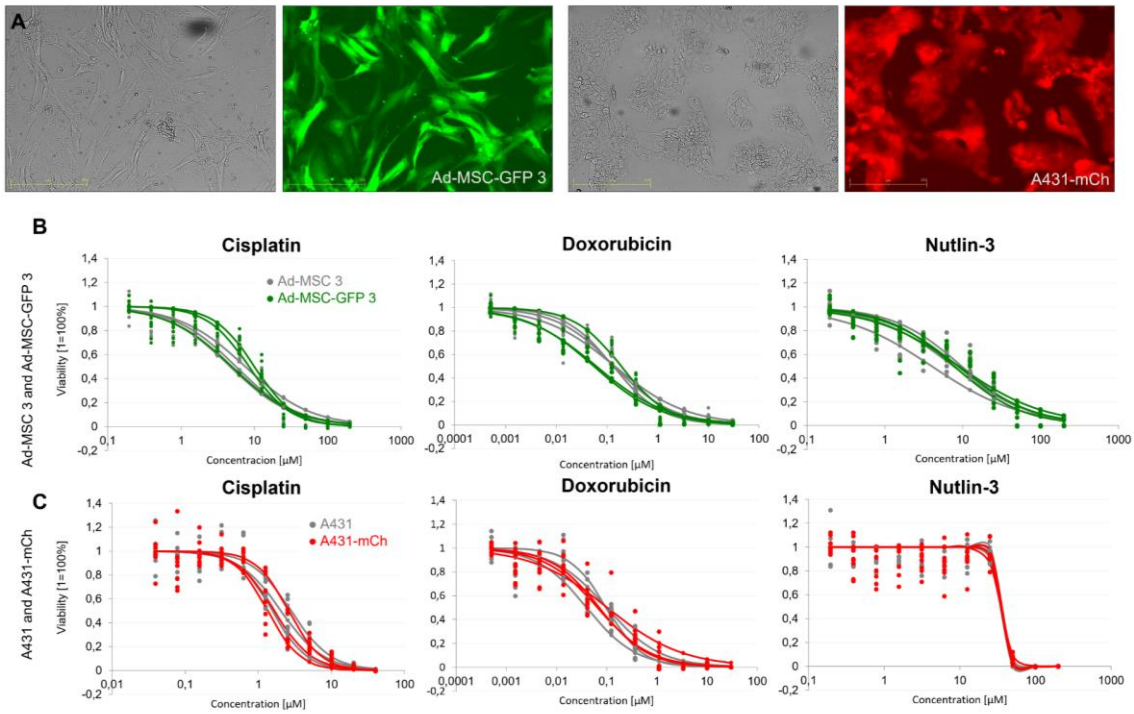


| D | Cisplatin | | Doxorubicin | | Nutlin-3 | |
|---|---|---|---|---|---|---|
| | $IC_{50}$ [µM] | st.dev. | $IC_{50}$ [µM] | st.dev. | $IC_{50}$ [µM] | st.dev. |
| Ad-MSC 3 | 7.873 | ± 2.545 | 0.136 | ± 0.863 | 8.321 | ± 1.140 |
| Ad-MSC-GFP 3 | 9.989 | ± 1.744 | 0.084 | ± 1.06 | 8.889 | ± 0.151 |
| A431 | 2.052 | ± 0.625 | 0.0727 | ± 0.033 | 33.802 | ± 7.325 |
| A431-mCh | 1.888 | ± 0.26 | 0.0780 | ± 0,019 | 33.885 | ± 1.2 |

***Figure 4.*** *Comparison of dose-response curves of GFP/mCherry expressing and parental cell lines. Brightfield and fluorescent image of morphology of Ad-MSC-GFP 3 and A431-mCh cells (A). Transduction and non-transduced cells cytotoxicity dose-response curves (B, C) and $IC_{50}$ values (D).*

### 4.3. Investigation of drug sensitivity with nine different compounds

Nine different clinically relevant compounds were tested on stem cell-like cell lines from healthy donors (Ad-MSC-GFP 1, 2, 3, BM-MSC and HFF) and on three different human

cancer cell lines (MCF-7: breast adenocarcinoma, MES-SA: uterine sarcoma and A431-mCh: skin epidermoid carcinoma,). Different chemotherapeutic agents were tested on different MSC-like cells from healthy human donors, a widely used breast cancer cell line (MCF-7), a mesenchymal gynecological (MES-SA) and an epidermal (A431) tumor type to investigate drug response. Nine chemotherapeutic agents with different mechanisms of action and structures were selected for analysis, including conventional and novel types of compounds that are also clinically used in cancer treatment: bendamustine (intrastrand crosslinker), cisplatin (interstrand crosslinker), doxorubicin (topoisomerase II inhibitor), irinotecan (topoisomerase I inhibitor), methotrexate (antimetabolite), mitoxantrone (topoisomerase II inhibitor), nutlin-3 (MDM2 inhibitor), TPEN (ion chelator) and vinblastine (anti-microtubule drug) were added in a defined dilution series (nine concentrations and one untreated condition) for 5 days (Table 2). On the basis of $IC_{50}$ values, three groups could be distinguished according to which compounds were more toxic to certain cell types.

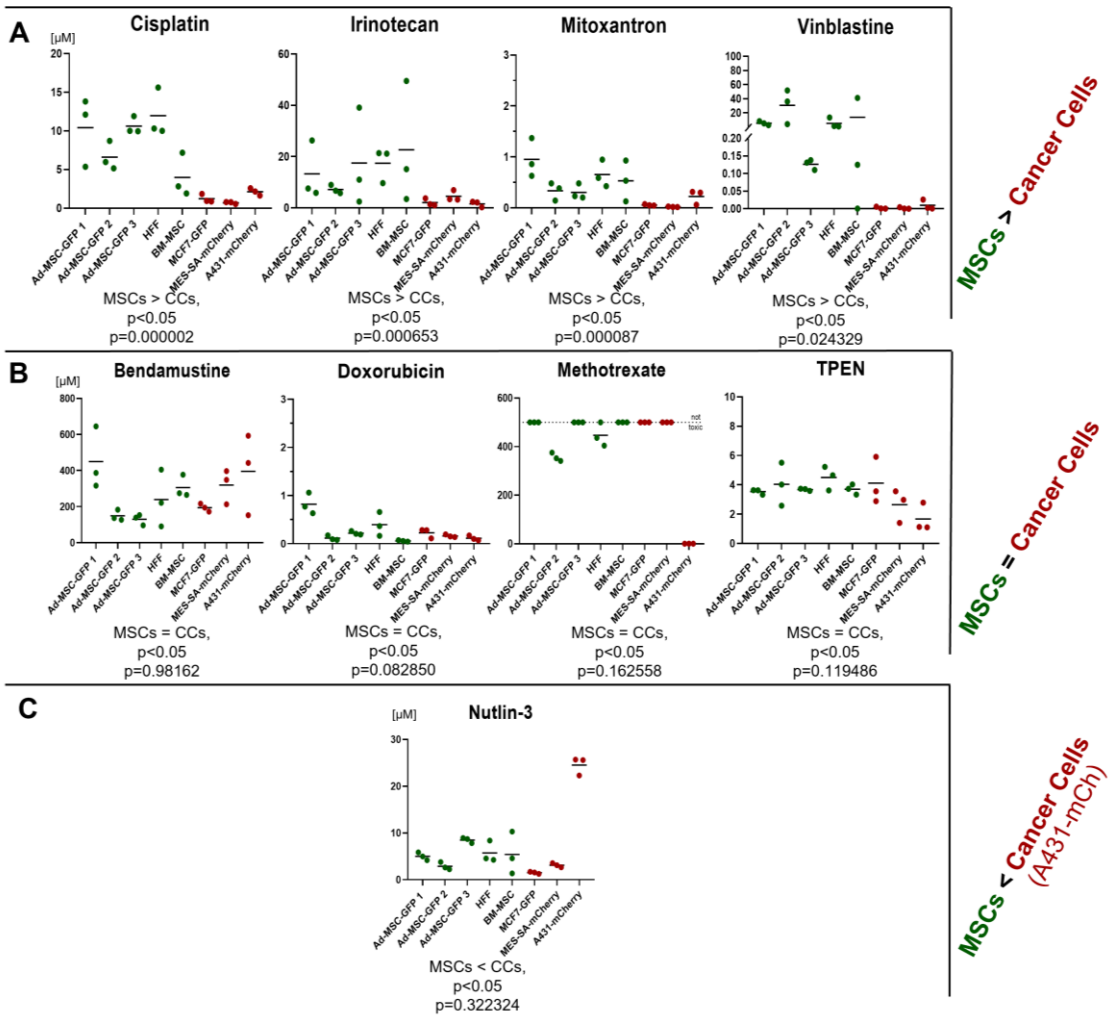


***Figure 5.*** *$IC_{50}$ values in -µM- concentration in all cell types. MSCs have higher drug tolerance to cisplatin, irinotecan, mitoxantrone and vinblastine (A). The F-test did not show significant differences in $IC_{50}$ values for bendamustine, doxorubicin, methotrexate and TPEN (B). Nutlin-3, which targets p53 wild type cells, whether is healthy or tumor cells. Only the A431-mCh cell line had higher sensitivity to nutlin-3 (C).*

The first group included compounds with higher $IC_{50}$ values in MSC cells than in tumor cells (MSCs > Cancer Cells) (Fig. 5 A). Generally speaking, chemotherapeutic agents work by killing cancer cells, with less effect on healthy cells in the body that are slowly circulating. In the middle group, no significant difference was found between $IC_{50}$ values, so the cells showed similar tolerability (MSCs = Cancer Cells) (Fig. 5 B). Nutlin-3 was placed in group 3 based on the mechanism of action, as only the $p53^{-/-}$ mutant A431-mCh cell was found to be resistant (MSCs < Cancer Cells (A431)) (Fig. 5 C). This compound

was developed for tumor types with wild-type p53 and it kills MCF-7-GFP and MES-SA-mCh as well as MSC-like cells.

Chemotherapeutics target tumor cells proliferate more rapidly than other types of cells in the body. On the basis of our drug sensitivity results, we investigated whether there was any difference between the proliferation rates of MSCs and tumor cells.

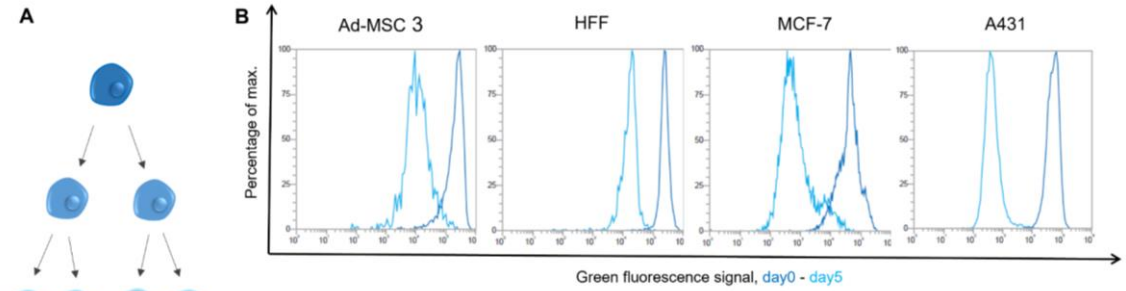


| C | Ad-MSC 3 | HFF | MCF-7 | A431 |
|---|---|---|---|---|
| Cell numbers | d0: 1.5 x $10^5$ | d0: 1.5 x $10^5$ | d0: 1.5 x $10^5$ | d0: 1.5 x $10^5$ |
| | d5: 7.5 x $10^5$ | d5: 9 x $10^5$ | d5: 25.5 x $10^5$ | d5: 33 x $10^5$ |
| Increase | **5x** ↑ | **6x** ↑ | **17x** ↑ | **22x** ↑ |

***Figure 6.*** *Comparison of cell division rate of two MSC-like cells (Ad-MSC 3 and HFF) and two cancer cells (MCF-7 and A431). The CytoTell™ cell tracking assay can show how a fluorescent non-toxic dye is diluted from the cells with each mitosis (A). Dark blue indicates the starting point (day 0), and light blue shows the fifth day (day 5). The gap between the two curves is larger for MCF-7 and A431 cells, indicating that tumor cells proliferate more rapidly than MSC-like cells (B). The table shows the increased cell number and the rate of the growth (C).*

As the CytoTell fluorescent dye is diluted out of the cells with each mitosis, the green fluorescent signal is lower in tumor cells (MCF-7 and A431) than in MSCs (Ad-MSC 3 and HFF), indicating that tumor cells proliferate faster than the MSCs (Fig. 6 B). Changes in cell number over five days also indicate that tumor cells have a higher proliferation rate (Fig. 6 C). Therefore, for some drugs, virtually identical tolerance (MSCs = Cancer Cells) cannot be explained by similar proliferation.

### 4.4. Live cell imaging

On the basis of our results for the tested nine compounds, we selected one representative compound from each of the three groups. We used live cell microscopy to see what morphological changes occurred during treatment with cisplatin, doxorubicin and

nutlin-3. Cells expressing GFP and mCherry and their response to drug treatment were monitored for 120 h. Concentrations were selected based on the effect on MSCs and tumor cells, so we generally treated cells with low, medium and high concentrations of cisplatin, doxorubicin, and nutlin-3 in 10-fold dilution series (Fig. 7 A).

The response of A431-mCh cells to drugs was as expected; both $IC_{50}$ and higher concentrations of doxorubicin and cisplatin significantly reduced the number of viable colonies, whereas lower concentrations of the drugs (0.2µM cisplatin and 0.01µM doxorubicin) did not change cell growth kinetics in comparison to untreated controls. Nutlin-3 had no effect on $p53^{-/-}$ A431-mCh cultures in either concentration because it was designed to specifically target p53 wild-type cells. Interestingly, no discernible reduction was seen in Ad-MSC-GFP 3 cultures following a 120-hour treatment, despite cytotoxicity data indicating that MSCs and cancer cells had a strikingly similar sensitivity to doxorubicin. The confluence of Ad-MSC-GFP 3 was significantly reduced only at high cisplatin (20µM) and nutlin-3 (3µM) concentrations (Fig. 7 A and B). This result suggests that MSCs follow a different route, such as cell cycle arrest, senescence or differentiation rather than disappearing after treatment and can only be eliminated at much higher concentrations than the $IC_{50}$ found in the cytotoxicity test.

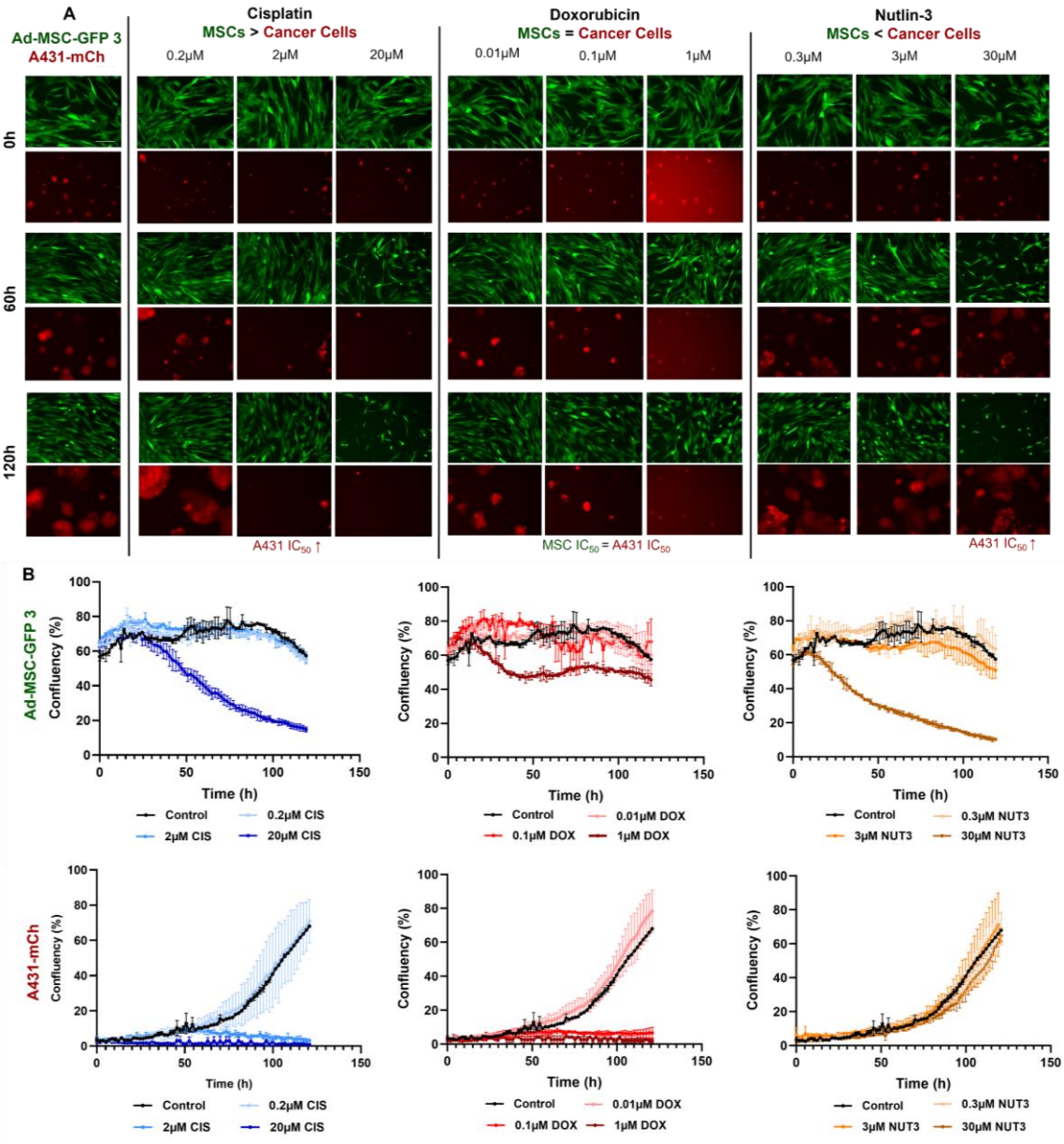


***Figure 7.*** *Image sequence of Ad-MSC-GFP 3 and A431-mCh cells at 0 h, 60 h and 120 h. Photographs were taken every 105 minutes for 120 h. To demonstrate the growth or the inhibition of the cultures, cells were treated with three different concentrations of cisplatin (0.2μM, 2μM, 20μM), doxorubicin (0.01μM, 0.1μM, 1μM) and nutlin-3 (0.3μM, 3μM, 30μM) (A). Please note that doxorubicin autofluorescence caused intense background fluorescence at 1μM. Image analysis was used to calculate changes in confluence (%) from three separate parallels. Confluence of MSCs starts higher (60%) because MSCs are larger than the A431-mCh cells. Top row: A431-mCherry cells*

*exposed to varying amounts of cisplatin, doxorubicin and nutlin-3; bottom row: Ad-MSC-3 GFP cells (B).*

### 4.5. DNA-damage and ROS induced in cells

As cisplatin, doxorubicin, and nutlin-3 can all cause DNA-damage and ROS in cells, we investigated the levels of double-strand breaks (DSB) and ROS in Ad-MSC-3/Ad-MSC-GFP 3 and A431/A431-mCh cell lines (Fig. 8.). Treatment concentrations were based on $IC_{50}$ values of the A431-mCh cells.

The number of DSB foci in MSCs was significantly lower with 2µM cisplatin (at the $IC_{50}$ value of A431-mCh cells), whereas A431 cells were nearly entirely eliminated by using the same concentration of cisplatin.

In A431-mCh cells, 0.1µM doxorubicin caused less DNA-damage than 2µM cisplatin, whereas MSCs DNA suffered less genetic mutation.

Nutlin-3, which did not reduce the number of A431-mCh cells after 120 hours of treatment based on live-cell imaging experiments, severely damaged the DNA. On the other hand, despite the fact that both cytotoxicity and video microscopy experiments showed significantly reduced viability in Ad-MSC-GFP 3 cells with 8µM nutlin-3, no DNA-break was found even after 30µM nutlin-3 treatment (Fig. 8. pink highlights).

As the evaluation of DNA damage did not explain the similarities in drug sensitivity, we wondered whether 1 hour of treatment with cisplatin, doxorubicin and nutlin-3 would induce ROS in the cells. Interestingly, only 30µM nutlin-3 generated considerable amounts of ROS in Ad-MSC 3 and A431 cells. On the basis of live-cell imaging, 30µM of nutlin-3 was more toxic to Ad-MSC-GFP 3 than A431, indicating that cancer cells may have a higher tolerance for ROS-induced damage (Fig. 8. green highlights). As a positive control, 130µM hydrogen-peroxide ($H_2O_2$) was used to validate DCFH-DA oxidation to green fluorescent DCF (data not shown).

However, as there was a significant difference in DNA damage in the two cell types, the drug sensitivity pattern could not be explained by the levels of the DNA double-stranded breaks or the ROS levels.

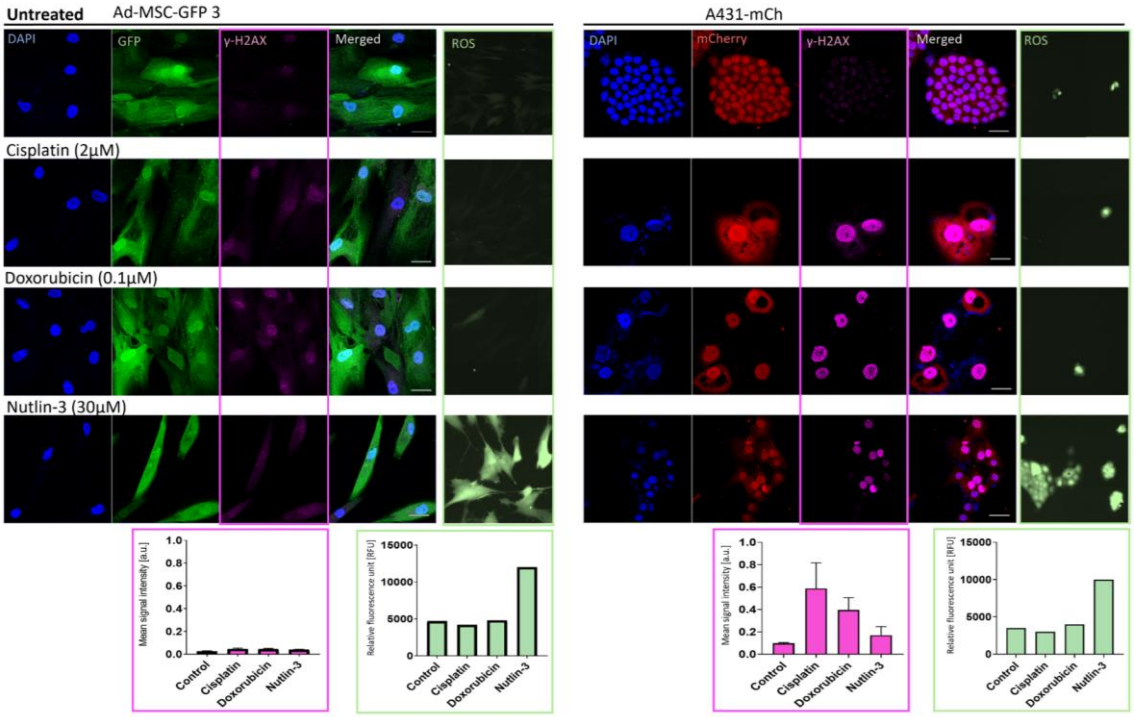


***Figure 8.*** *Immunostaining of gamma-H2AX, quantification of DSB and ROS-detection in Ad-MSC 3/Ad-MSC-GFP 3 and A431/A431-mCh cells. After 120 hours of treatment with cisplatin and doxorubicin, most of the tumor cells detached due to the high DNA-damage, but in contrast, MSCs suffered fewer DNA double-stranded breaks. Nutlin-3 treatment caused DNA-damage only in A431-mCh cells, but increased ROS in both cell types. Please note that DNA damage and ROS staining were two separate experiments.*

### 4.6. Apoptosis

Chemotherapy is aimed at inducing apoptosis of cancer cells, so we investigated how 120 hours of treatment with cisplatin, doxorubicin, or nutlin-3 affected the apoptotic pathways in cells. A431 cells showed apoptosis after all treatments and only a modest response to 30μM nutlin-3. No apoptosis was observed in MSCs during the experiments, even when drug concentrations were increased, sometimes 10-fold. Doxorubicin caused apoptosis in almost all A431 cells, but not in Ad-MSC 3 cultures. Treatment with 30μM nutlin-3 only slightly increased the number of apoptotic MSCs, whereas cisplatin caused virtually no apoptosis compared to untreated controls (Fig. 9.).

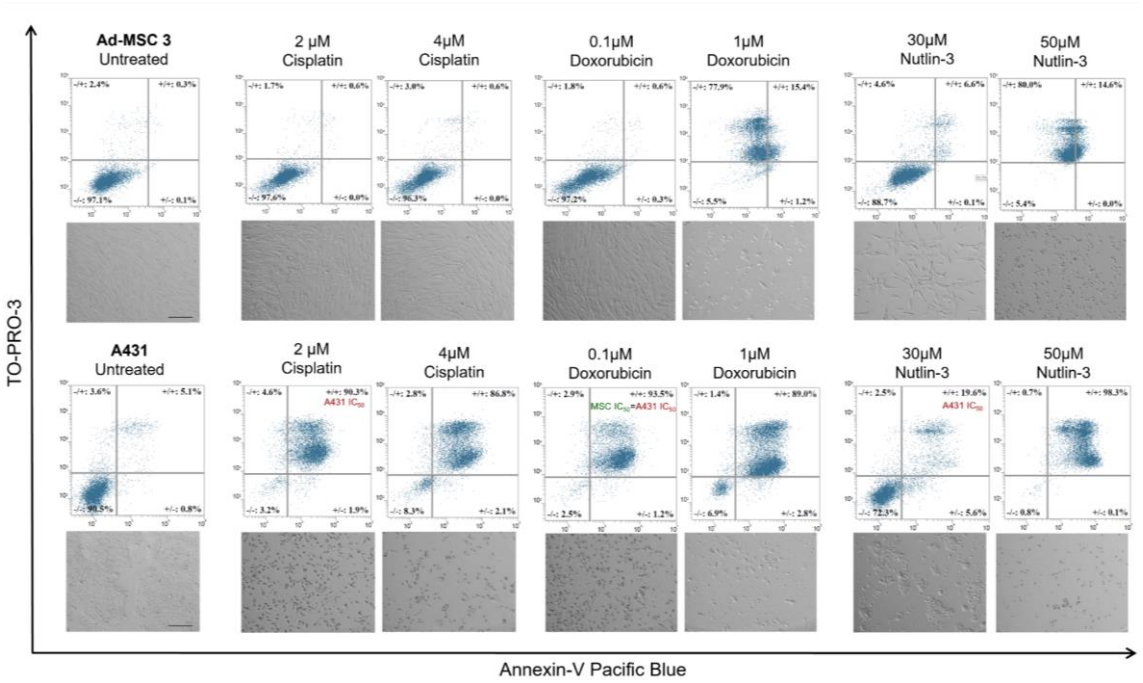


***Figure 9.*** *Apoptosis detection with double staining using Annexin-V Pacific Blue and TO-PRO-3. Tumor cells respond to most treatments by apoptosis, whereas 30µM nutlin-3 was the only treatment that did not kill a significant proportion of cancer cells. Ad-MSC- cells did not activate apoptotic pathways in higher doses of treatment with doxorubicin (1µM) and nutlin-3 (50µM). Scale bars represent 200µm.*

### 4.7. Senescence

Senescence, a type of permanent exit from the cell cycle, can also be induced by chemotherapeutic treatment. This occurs when cells are arrested in the $G_0$ phase. Senescence-associated β-galactosidase (SA-β-Gal) staining identifies increased β-galactosidase enzyme activity in cells that are usually elevated in senescent cells. Only 4µM cisplatin-treated MSCs show mild senescence positivity (blue color), the other treatments did not induce senescence in either Ad-MSC 3 or A431 cells (Fig. 10 A). However, doxorubicin exposure reduced the number of cells in the MSC population, destroyed most cancer cells, and slowed down proliferation in both cell lines (dark blue to light blue curves, dark blue to red curves) (Fig. 10 B and C).

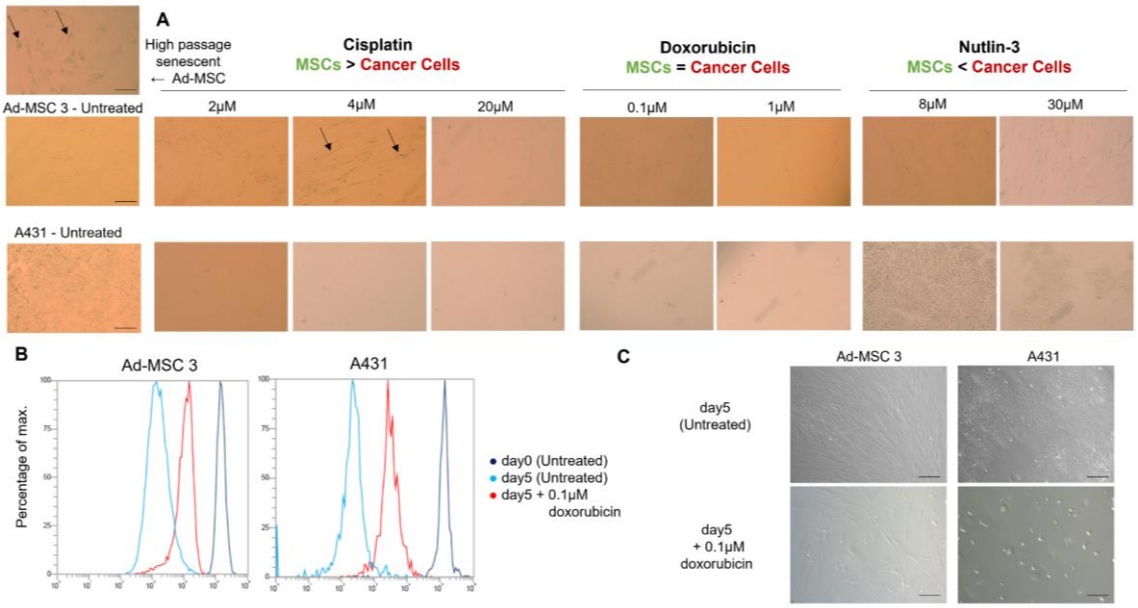


***Figure 10.*** *Senescence-associated ß-galactosidase (SA-ß-Gal) staining in Ad-MSC 3 and A431 cells. Senescent Ad-MSC 3 cells at high passage number were used as positive controls, only 4μM cisplatin showed a slight positivity for senescence staining (A). CytoTell assay shows how the green fluorescent signal is diluted from the cells with every cell division after five days of 0.1μM doxorubicin treatment (B). Morphological changes after doxorubicin treatment (C).*

### 4.8. Cytokines secreted by cells and their changes in co-culture

We investigated the secretion of 36 cytokines and chemokines in 2D mono- and co-cultures of Ad-MSC-GFP 3 and A431-mCh cells (Fig. 11 A). It was found that the initial number of Ad-MSC-GFP 3 cells increased more than 3-fold in monocultures after 5 days, while the number of A431-mCh cells increased nearly 20-fold under the same conditions. Co-cultures showed similar increases of 2.5- and 16-fold, allowing the comparison of cytokine profiles between mono- and co-cultures (Fig. 11 B).

We found that only 9 of the 36 cytokines-chemokines could be detected in the model, and the two cell lines showed slightly similar secretion profiles. Both MSCs and A431 cells secreted SERPINE1/PAI-1, IL-8, and CXCL1/GROα, while CCL2/MCP1, IL-6 was only found in MSC cultures and CCL5/RANTES, MIF, GM-CSF and ICAM-1/CD54 were only detected in supernatants of cancer cells. MSCs are known to produce a complete arsenal of cytokines, chemokines, which was highly evident when pixel intensity was normalized to cell number on day 5. The similarity of the secreted cytokines in the two

cell lines is surprising, but the results from co-cultures suggest a remarkable interaction between MSCs and cancer cells. SERPINE1/PAI-1, was strongly secreted by MSCs but could be hardly detected in A431-mCh cells and in co-cultures. Surprisingly, the expression level of CCL2/MCP-1 was drastically increased, its expression was virtually stimulated in co-cultures. CCL5/RANTES, a chemokine receptor overexpressed in hematological and solid tumors, was found at low levels in A431 cells but decreased in co-cultures. IL-6 was detected in small amounts in MSCs and virtually absent from A431 cultures but increased in co-cultures. CXCL1/GROα levels were reduced in co-cultures without further effects on secretion. Changes in MIF, GM-CSF and ICAM-1/CD54 levels were not significant (Fig. 11 C). The role of cytokines is summarized in Table 3.

***Table 3:*** *Function of secreted cytokines and chemokines*

| Name | Function | Ref. |
|---|---|---|
| **SERPINE1/ PAI-1** | **Serine Proteinase Inhibitor 1/ Plasminogen Activator Inhibitor-1**<br>regulation of ECM degradation,<br>inhibition of plasminogen to plasmin cleavage,<br>tumor cells growth and invasiveness induction | (60)<br>(61) |
| **CCL2/ MCP1** | **C-C Motif Chemokine Ligand 2/ Monocyte Chemoattractant Protein-1**<br>pro-inflammatory cytokine, recruitment of immune cells,<br>repolarization of macrophages, cell migration and chemoattraction | (62)<br>(63) |
| **CCL5/ RANTES** | **C-C Motif Chemokine Ligand 5/ Regulated on Activation, Normal T-cell Expressed and Secreted**<br>pro-inflammatory cytokine, tumor cell invasion,<br>activation of MMPs | (64) |
| **IL-6** | **Interleukin-6**<br>pro-and anti-inflammatory cytokine,<br>immunosuppression, tissue regeneration | (65)<br>(66) |
| **IL-8** | **Interleukin-8**<br>pro-angiogenic, cell attractant,<br>cell division and migration promoter | (67) |
| **CXCL-1/ GROα** | **C-X-C motif ligand-1/Growth Regulated Oncogene alpha**<br>pro-angiogenic and tumor formation cytokine | (68) |
| **MIF** | **Macrophage migration Inhibitory Factor**<br>pro-angiogenic, inhibition of apoptosis, cell survivor | (69) |
| **GM-CSF** | **Granulocyte-Macrophage Colony-Stimulating Factor**<br>increases self-migration, promotes aggressiveness of cancer cell | (70)<br>(71) |
| **ICAM/ CD54** | **Intercellular Adhesion Molecule 1/ Cluster of Differentiation 54**<br>recruition of immune cells, tissue regeneration,<br>increase self-migration | (72)<br>(73) |

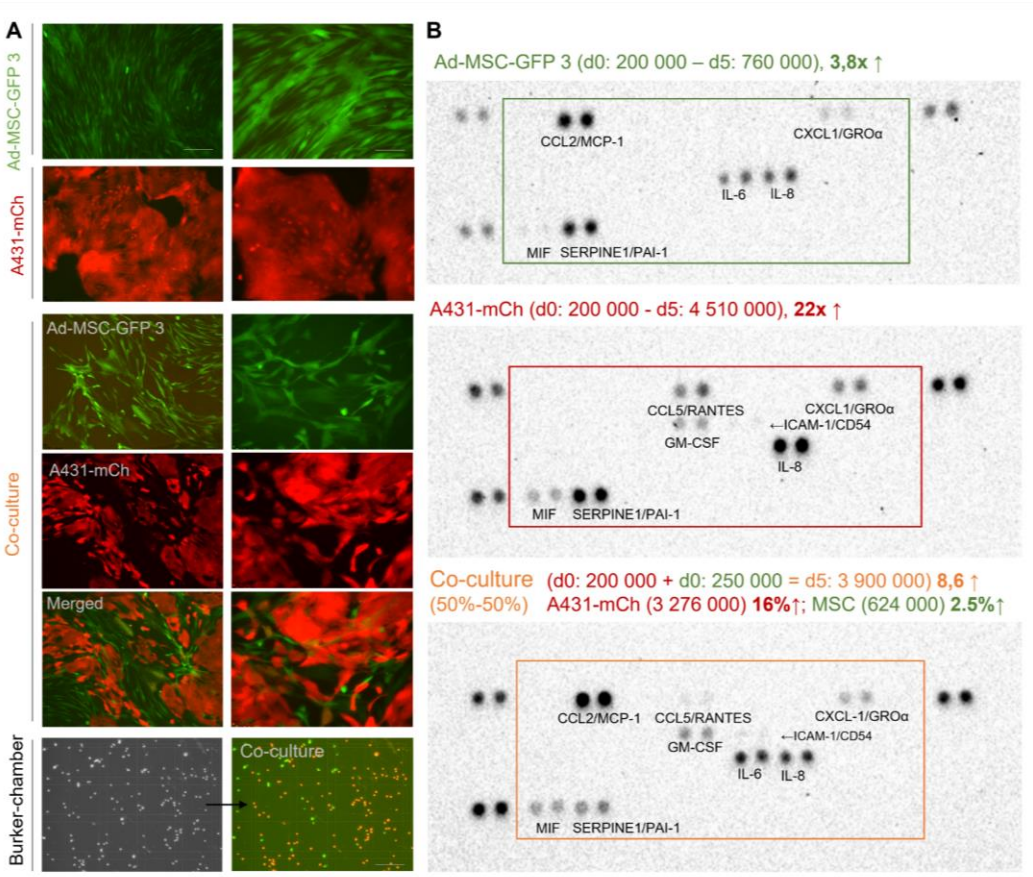
A
Ad-MSC-GFP 3
A431-mCh
Co-culture
Ad-MSC-GFP 3
A431-mCh
Merged
Burker-chamber
Co-culture
B
Ad-MSC-GFP 3 (d0: 200 000 – d5: 760 000), 3,8x ↑
CCL2/MCP-1
CXCL1/GROα
IL-6
IL-8
MIF
SERPINE1/PAI-1
A431-mCh (d0: 200 000 - d5: 4 510 000), 22x ↑
CCL5/RANTES
CXCL1/GROα
←ICAM-1/CD54
GM-CSF
IL-8
MIF
SERPINE1/PAI-1
Co-culture (d0: 200 000 + d0: 250 000 = d5: 3 900 000) 8,6 ↑
(50%-50%) A431-mCh (3 276 000) 16%↑; MSC (624 000) 2.5%↑
CCL2/MCP-1
CCL5/RANTES
CXCL-1/GROα
←ICAM-1/CD54
GM-CSF
IL-6
IL-8
MIF
SERPINE1/PAI-1

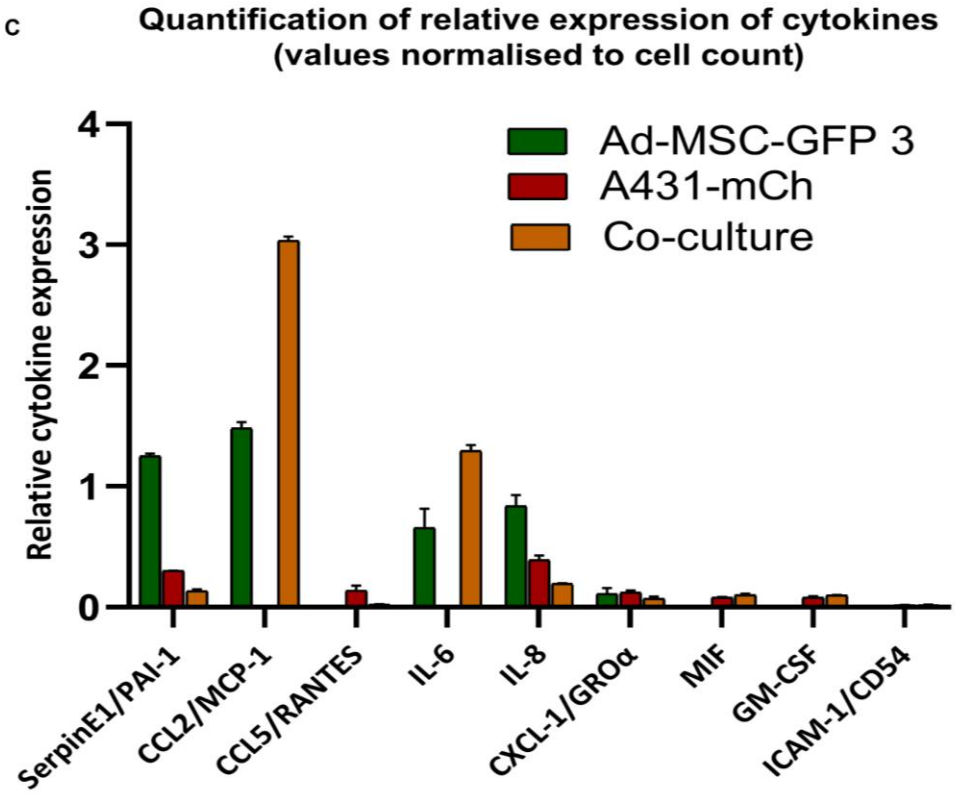
C
Quantification of relative expression of cytokines
(values normalised to cell count)
Relative cytokine expression
0
1
2
3
4
Ad-MSC-GFP 3
A431-mCh
Co-culture
SerpinE1/PAI-1
CCL2/MCP-1
CCL5/RANTES
IL-6
IL-8
CXCL-1/GROα
MIF
GM-CSF
ICAM-1/CD54

***Figure 11***. *Secretion profile of cytokines in 2D MSC, cancer cells and co-cultures. Fluorescence images of Ad-MSC-GFP 3 and A431-mCh tumor cells and co-culture at 10- and 20-fold magnification. Co-cultured cell count was determined using a Burker-chamber under fluorescent microscope (A). Detection of levels of multiple cytokines Ad-MSC-GFP 3, A431-mCh cells and co-culture samples (B). Evaluation of cytokine secretion levels by analyzing the intensity of positive dots and values was normalized to cell number on day 5 (C). Scale bar is 200µm in the left panel and 100µm in the right panel.*

### 4.9. Effect of chemotherapeutics on 2D mono- and co-cultures

It raises the question whether or not the presence of MSCs alters A431-mCh cell sensitivity. As the PrestoBlue assay cannot separate two cell lines in co-culture, we used mCherry fluorescence of tumor cells to measure viability. We examined changes in drug sensitivity by mixing the cells in a ratio of 50% each, but found no differences, dose-response curves overlapped according to the endpoint analysis on day 5 (Fig. 12.).

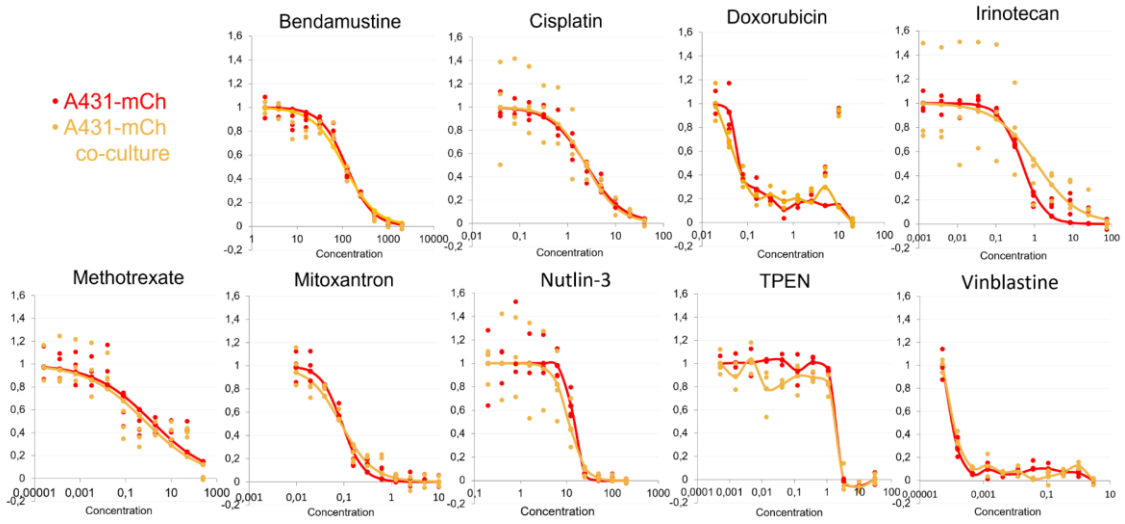


***Figure 12.*** *No shift in drug sensitivity of A431-mCh cells was observed in co-culture after 120 h. A431-mCh (red) and co-cultured A431-mCh (orange) dose-response curves overlapped.*

As a consequence, our investigations were extended to different proportions of MSCs and tumor cells on a wider scale. To investigate the effects of co-culture in more detail, we

combined different proportions of tumor cells and MSCs, modeling a low, a moderate or a highly stromal tumor TME:

➤ 20% Ad-MSC-GFP 3 - 80% A431-mCh,

➤ 50% Ad-MSC-GFP 3 - 50% A431-mCh,

➤ 80% Ad-MSC-GFP 3 - 20% A431-mCh.

We investigated the growth kinetics of different cell mixtures, answering how fast cells grow or die in monoculture, co-culture and in response to chemotherapeutic treatment. On the basis of previous experiments, cisplatin and nutlin-3 were selected from the compound panel for further experiments; thus, there was one compound that targeted MSCs (nutlin-3) and one compound that targeted tumor cells (cisplatin). Tumor cells were significantly destroyed by 10µM cisplatin, which is equivalent to the $IC_{50}$ of MSCs. Cisplatin killed tumor cells in a dose-dependent manner, but in co-culture, the presence of MSCs did not change the growth kinetics of tumor cells, so they did not grow faster and did not develop cisplatin resistance (Fig. 13 A and B). Nutlin-3 was more effective in killing MSCs, but tumor cells did not grow more rapidly, and no resistance developed. The heat map fitted to the endpoint values of the growth curves shows a relative comparison of the confluence values of MSCs and tumor cells. Thus, taking the confluence values of untreated MSCs and A431-mCh cells on day 5 as 100%, shows how confluence changes with cisplatin and nutlin-3 treatment compared to this in % (Fig. 13 C). Therefore, it was found that co-culturing did not alter cisplatin or nutlin-3 sensitivity of A431-mCh cells in different MSC and cancer cell ratios. No significant differences in toxicity were observed between mono- and co-cultures in 2D.

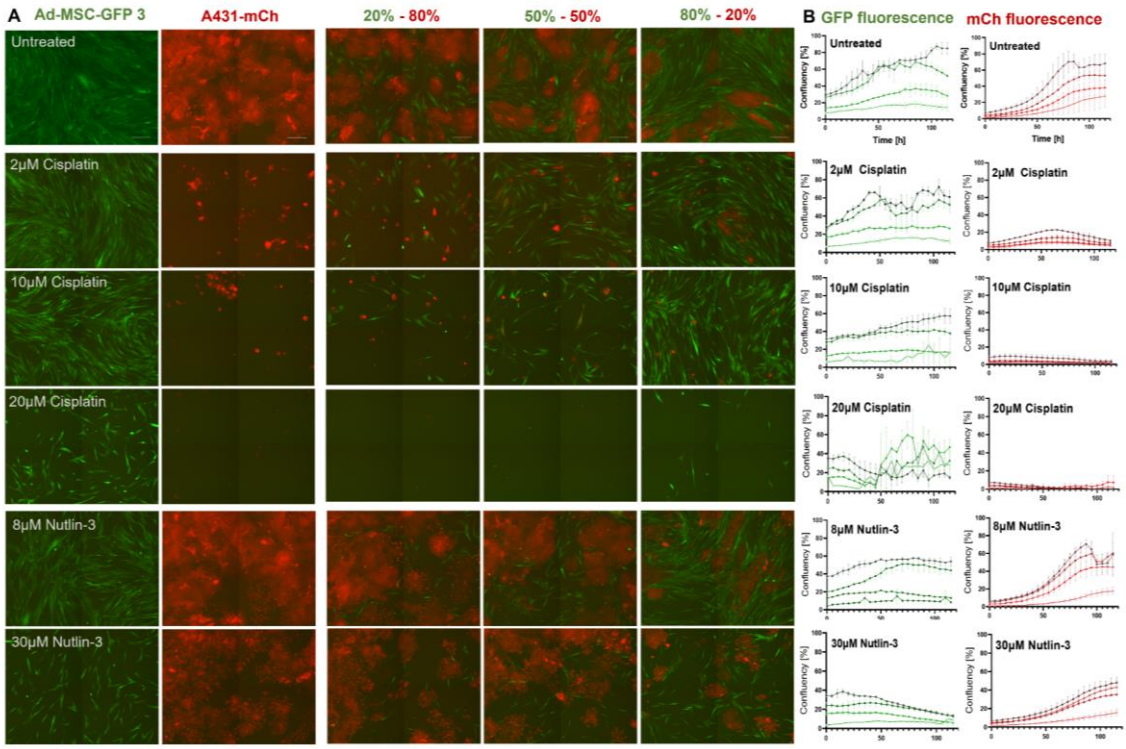


C

live dead

live dead

Legends for panel B:

- Ad-MSC-GFP 3 Control
- 20% A431-mCh - 80% Ad-MSC-GFP 3 GFP
- 50% A431-mCh - 50% Ad-MSC-GFP 3 GFP
- 80% A431-mCh - 20% Ad-MSC-GFP 3 GFP
- A431-mCh Control
- 80% A431-mCh - 20% Ad-MSC-GFP 3 mCh
- 50% A431-mCh - 50% Ad-MSC-GFP 3 mCh
- 20% A431-mCh - 80% Ad-MSC-GFP 3 mCh

| 2D | A431 | 80% tumor | 50% tumor | 20% tumor | MSC | 20% MSC | 50% MSC | 80% MSC |
|---|---|---|---|---|---|---|---|---|
| Untreated | 100,0 | 77,3 | 55,6 | 40,3 | 100,0 | 16,6 | 33,2 | 61,3 |
| 2μM cisplatin | 15,2 | 10,6 | 7,1 | 7,9 | 71,8 | 14,6 | 31,1 | 61,7 |
| 10μM cisplatin | 5,2 | 2,9 | 3,0 | 1,4 | 67,4 | 19,9 | 19,7 | 44,5 |
| 20μM cisplatin | 0,4 | 0,2 | 2,7 | 3,6 | 17,6 | 32,7 | 55,1 | 38,5 |
| 8μM nutlin-3 | 85,5 | 87,6 | 64,9 | 25,6 | 63,6 | 9,8 | 15,4 | 51,7 |
| 30μM nutlin-3 | 69,7 | 51,1 | 62,1 | 22,8 | 15,7 | 10,4 | 6,9 | 14,9 |

***Figure 13.*** *Effects of cisplatin and nutlin-3 on 2D MSC, A431 and co-cultures. Endpoint images of 2μM, 10μM and 20μM cisplatin and 8μM and 30μM nutlin-3 treatment in 2D mono-and*

*co-cultures. Scale bar represents 250μm (A). Cells were imaged every 5 h for 120 h. Growth kinetics were plotted on the graphs for MSC (green) and A431-mCh (red) (B). The heat map fitted to the endpoint analysis of growth kinetics shows that tumor cells did not grow faster and did not develop resistance (C).*

### 4.10. MSCs provide an inner scaffold for cancer cells in 3D co-culture spheroids

For TME modeling, 2D studies did not yield any results; therefore, we considered developing a more relevant 3D TME model system. In order to gain a more precise insight into key aspects of TME and architecture/stratification, we established 3D spheroids using different ratios of MSCs and cancer cells as described above (20%-80%, 50%-50%,

80%-20%). We observed that the spheroid co-cultures were organized into the same structure, with MSCs and cancer cells separated into an MSC-core and a cancer cell outer layer. We took confocal images of the spheroids and reconstructed the 3D structure, suggesting MSCs provide an inner feeder-core to cancer cells. However, after 5 days, the size of the spheroids cultured in mono-culture slightly shrank, probably due to cell death or spheroid compaction. Co-cultured spheroids did not change significantly in size (Fig. 14.).

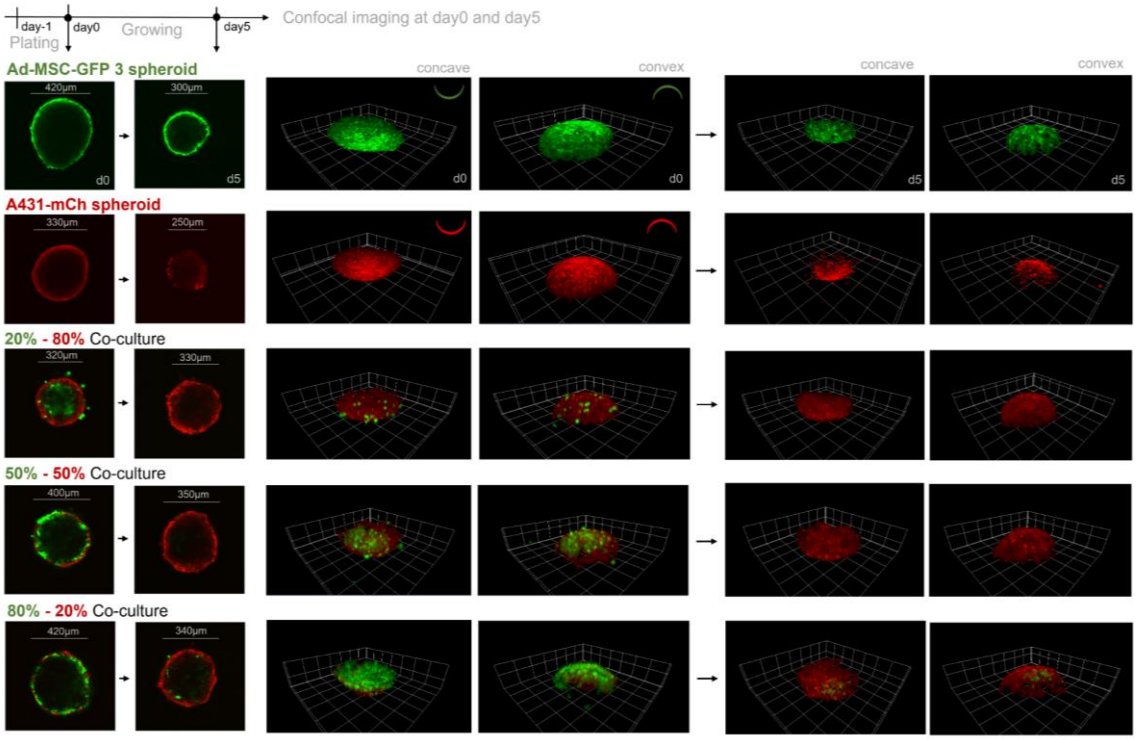


***Figure 14.*** *Internal organization of 3D spheroids from Ad-MSC-GFP 3 and A431-mCh cells in different compositions. The 3D co-cultures of Ad-MSC-GFP 3 cells and A431-mCh cells show a consistent pattern, with A431-mCh spheroids surviving on the surface of MSCs despite varying initial MSC-cancer cell ratios.*

### 4.11. MSCs in 3D co-cultures enhance the drug tolerance of cancer cells

In 2D cultures, MSCs had no impact on the drug sensitivity of cancer cells as described above (Chap. 4.9. and Fig. 13.), thus establishing a 3D spheroid co-culture system where further analysis and toxicity experiments could be performed. In 3D mono-cultures, both MSC and A431 spheroids were slightly reduced in size over time and their growth curves

declined (Fig. 15 A and B). Surprisingly, co-cultured cancer cells not only avoided size reduction, but also increased growth kinetics and proliferation (Fig. 15 A and B). Interestingly, the fluorescence intensity curves of tumor cells only increase when co-cultured with MSCs, otherwise they show a decreasing trend. A heat map was fitted to the endpoints of the growth kinetics, similarly to the 2D studies. Surprisingly, while 2µM cisplatin killed A431 cells in 2D cultures and spheroid mono-cultures, cancer cells proliferated at 10µM in 3D co-cultures. In contrast, 10µM cisplatin was toxic to Ad-MSC spheroids, unlike in 2D cultures. Treatment with 20µM cisplatin had a similar effect on Ad-MSC and co-culture spheroids, but A431-mCh cells persisted in 20% to 80% of co-cultures, indicating altered drug sensitivity induced by MSCs despite being affected. This observation is in agreement with the results of 30µM nutlin-3 treatment, where Ad-MSCs were killed in all conditions, yet the dying cells provided substantial support for A431 cell growth compared to mono-culture conditions. Notably, cancer cells survived higher cisplatin concentrations, suggesting that the protective effect of MSCs was not based on the physical arrest of A431 cells. TO-PRO-3 staining revealed the presence of dead cells in spheroids as a function of GFP and mCherry expression (Fig. 15 C). Flow cytometric analysis of six spheroids further supported these findings (Fig. 15 C and D).

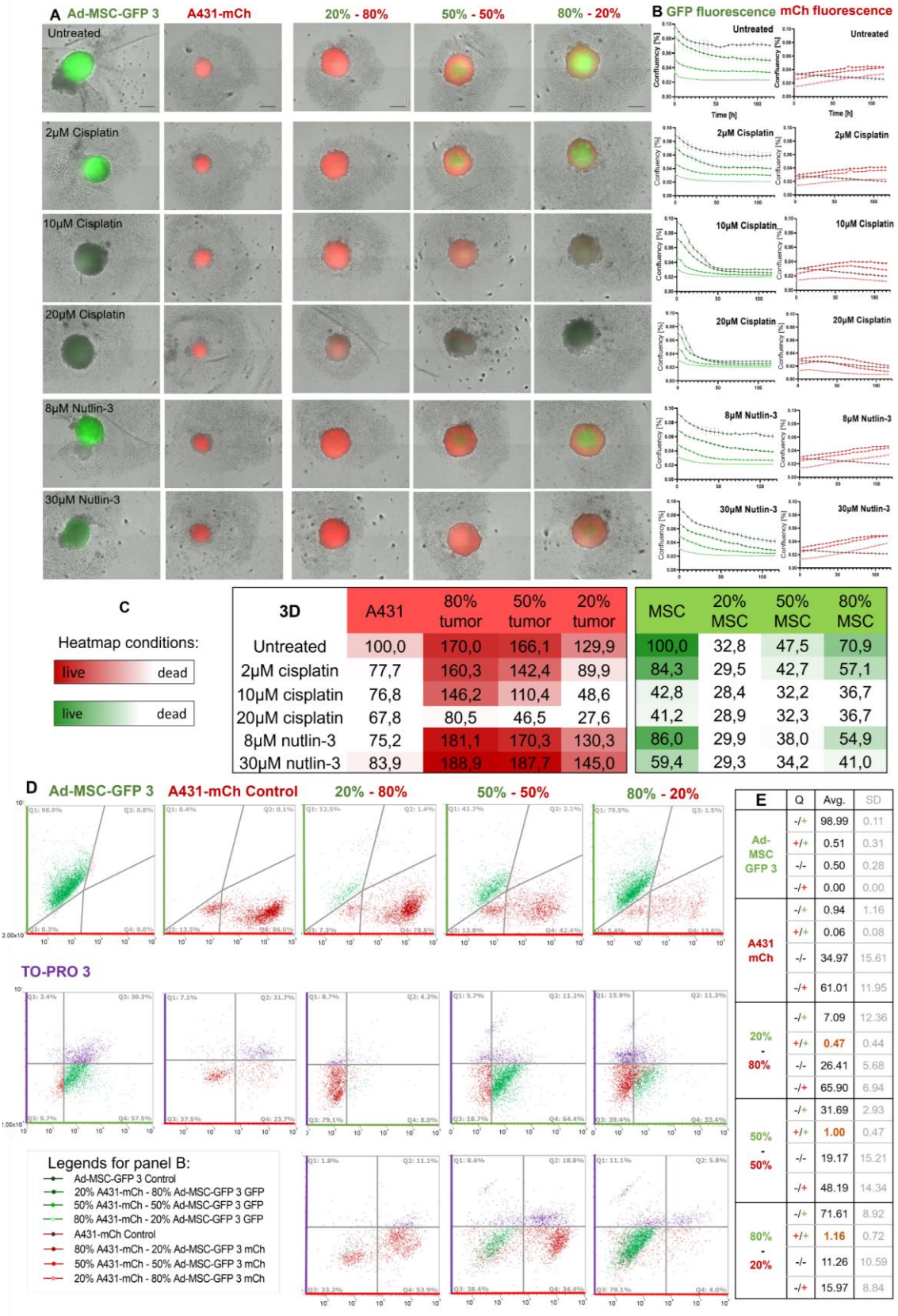


| 3D | A431 | 80% tumor | 50% tumor | 20% tumor |
|---|---|---|---|---|
| Untreated | 100,0 | 170,0 | 166,1 | 129,9 |
| 2μM cisplatin | 77,7 | 160,3 | 142,4 | 89,9 |
| 10μM cisplatin | 76,8 | 146,2 | 110,4 | 48,6 |
| 20μM cisplatin | 67,8 | 80,5 | 46,5 | 27,6 |
| 8μM nutlin-3 | 75,2 | 181,1 | 170,3 | 130,3 |
| 30μM nutlin-3 | 83,9 | 188,9 | 187,7 | 145,0 |

| MSC | 20% MSC | 50% MSC | 80% MSC |
|---|---|---|---|
| 100,0 | 32,8 | 47,5 | 70,9 |
| 84,3 | 29,5 | 42,7 | 57,1 |
| 42,8 | 28,4 | 32,2 | 36,7 |
| 41,2 | 28,9 | 32,3 | 36,7 |
| 86,0 | 29,9 | 38,0 | 54,9 |
| 59,4 | 29,3 | 34,2 | 41,0 |

| E | Q | Avg. | SD |
|---|---|---|---|
| Ad-MSC GFP 3 | -/+ | 98.99 | 0.11 |
| | +/+ | 0.51 | 0.31 |
| | -/- | 0.50 | 0.28 |
| | -/+ | 0.00 | 0.00 |
| A431 mCh | -/+ | 0.94 | 1.16 |
| | +/+ | 0.06 | 0.08 |
| | -/- | 34.97 | 15.61 |
| | -/+ | 61.01 | 11.95 |
| 20% - 80% | -/+ | 7.09 | 12.36 |
| | +/+ | 0.47 | 0.44 |
| | -/- | 26.41 | 5.68 |
| | -/+ | 65.90 | 6.94 |
| 50% - 50% | -/+ | 31.69 | 2.93 |
| | +/+ | 1.00 | 0.47 |
| | -/- | 19.17 | 15.21 |
| | -/+ | 48.19 | 14.34 |
| 80% - 20% | -/+ | 71.61 | 8.92 |
| | +/+ | 1.16 | 0.72 |
| | -/- | 11.26 | 10.59 |
| | -/+ | 15.97 | 8.84 |

***Figure 15.*** *Endpoint images of 3D co-cultured A431-mch and Ad-MSC-GFP 3 cells in different ratios, treated with 2μM, 10μM, 20μM cisplatin and 8μM, 30μM nutlin-3. Cells*

*were imaged every 5 hours, creating a record of 120 hours (A), and growth curves were plotted by intensity analysis of GFP and mCherry fluorescence at each point (B). The same heat map setup was used as in Fig. 11 C. The scale bar represents 250µm. FACS analysis of mono-cultured and co-cultured spheroids, dead cells were stained with TO-PRO-3. The percentage of dead cells is shown by the correlation between GFP-TO-PRO-3 and mCh-TO-PRO-3 (C). Quadrants measured in percentage by flow cytometry (D).*

### 4.12. Rare double fluorescence ($GFP^+$ and $mCh^+$) cells in co-cultures

The study conducted flow cytometry studies on co-cultures and found a unique mCherry - GFP double fluorescent cell population. These cells were multi-nucleated and larger than A341 cells, suggesting that they were likely to be derived from the MSC compartment (Fig. 16 A). The same was confirmed by the FSC- SSC flow cytometry analysis, which can be described as MSCs in terms of size scatter and granularity (Fig. 16 A and B). Phalloidin staining revealed changes in morphology, size, and stress fibers in the cells, indicating the altered cell shape (Fig. 16 C). This finding supports the previous research by Liu et al, who observed that flow cytometric analysis revealed yellowish fluorescent hybrid cells with binucleated morphology. The double fluorescent cells showed a higher morphology than naive MSCs after reseeding and were formed by spontaneous cell fusion (74).

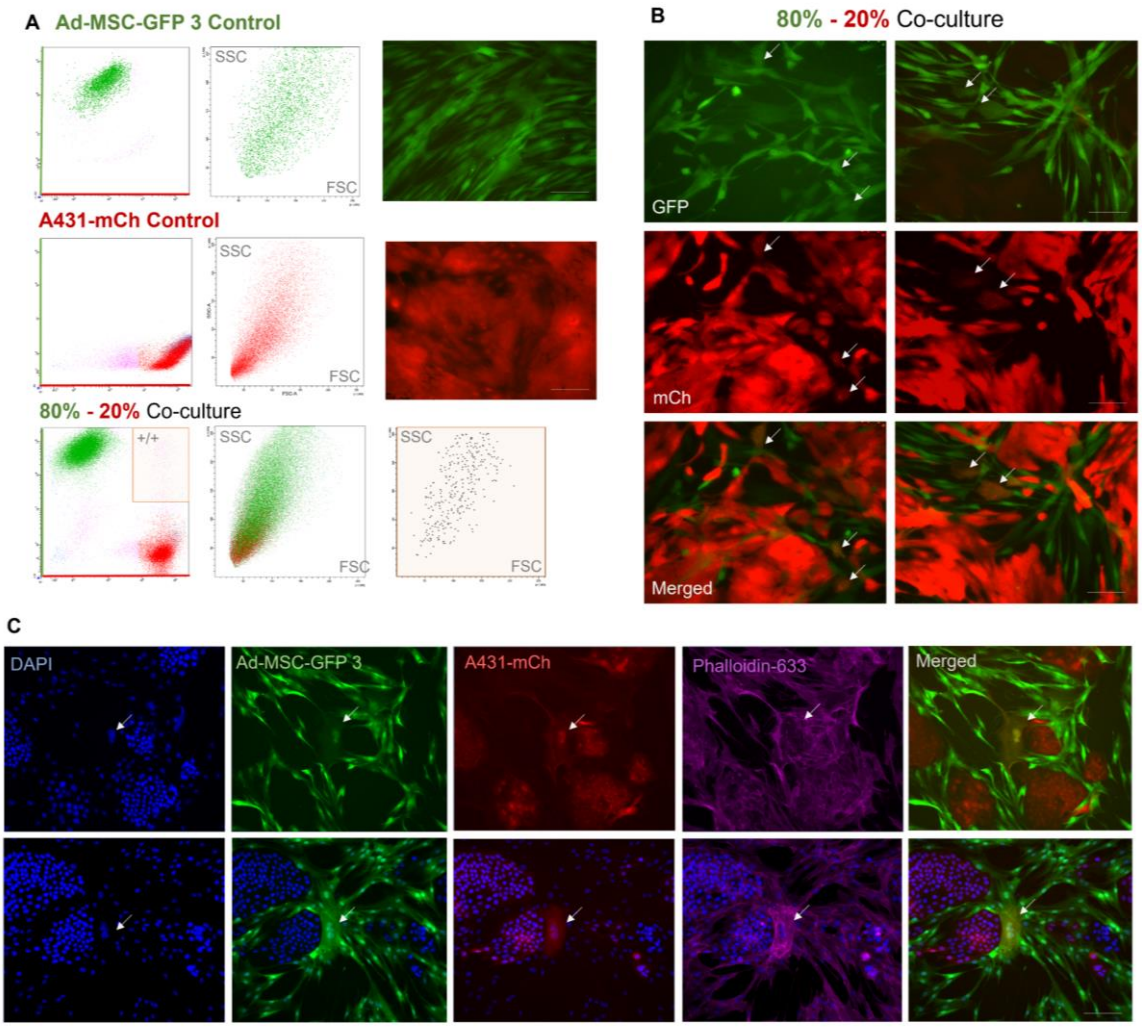


***Figure 16.*** *Examination of GFP$^+$ and mCh$^+$ cells by flow cytometry and microscopy. Flow cytometric analysis of control Ad-MSC-GFP 3 and A431-mCh cells (A). A double fluorescent, positive to GFP and mCh cell population appeared under co-culture conditions. Dual culture validation under fluorescent microscope (B). F-actin cytoskeletal component was stained with Phalloidin-633 in co-culture. White arrows show double fluorescent (GFP and mCherry) cells. These cells were found to be bi-or multinucleated and positive for actin staining (C). The scale bar represents 200μm.*

# 5. Discussion

Our main goal was to investigate the role of mesenchymal stem cells (MSCs) in cancer drug resistance, first by comparing how MSCs and cancer cells react to several clinically used compounds separately, and then how they influence each other's survival and drug tolerance when cultured together in 2D and 3D.

Despite being one of the most prevalent cell types in the tumor microenvironment (TME), the response of MSCs to chemotherapy remains largely unexplored. Prior to our work, MSCs had not been subjected to comprehensive drug sensitivity assessment (75). Our research aimed to compare the drug sensitivity of six MSC lines derived from individuals without cancer with three commonly studied cancer cell lines. We evaluated the response of these cells to nine distinct compounds that varied in structure and mechanism, and focused on three of them for a more detailed analysis.

MSCs showed remarkable resilience, often up to 10 000-fold, to DNA intercalation (cisplatin), inhibition of topoisomerases I and II (irinotecan and mitoxantrone), and disruption of microtubules (vinblastine) during screening. These findings are consistent with previous studies by other researchers who also tested these compounds on MSCs. Nicolay et al. demonstrated that MSCs derived from bone marrow (BM) and differentiated fibroblasts showed resistance to irinotecan and etoposide, most likely to be due to their efficient DNA repair mechanisms (76). Both Mueller and Liang et al. discovered that MSCs from bone marrow and adipose tissue show resistance to cisplatin, vincristine, and camptothecin, and also recover rapidly after exposure to these drugs (77, 78). It is commonly understood that chemotherapy specifically targets rapidly dividing cancer cells, which has a lesser effect on healthy tissues. This is due to the fact that quiescent and slowly cycling normal cells have lower levels of active DNA synthesis and other proliferation-related activities that are typically targeted by chemotherapeutic agents (79, 80). Given that MSCs proliferate at a significantly slower rate, this observed resistance can be explained.

Contrary to the prevailing belief in the scientific literature that mesenchymal stem cells (MSCs) are resistant to chemotherapy, our experiments have yielded remarkable findings that challenge this notion.

Surprisingly, four different chemotherapeutic compounds showed significant effectiveness against all cell lines, with no discernible benefit for MSCs over cancer cells. The compounds, including bendamustine for intrastrand crosslinking, doxorubicin for topoisomerase II inhibition, TPEN for inducing ROS damage, and the antimetabolite methotrexate affected MSCs in a manner similar to cancer cells.

While previous studies did not directly test bendamustine on MSCs, conflicting results have been reported, suggesting potential negative effects on stem cell mobilization in patients. However, low toxicity has been observed in vitro in hematopoietic stem cell cultures (81).

Some studies have found that doxorubicin and mitoxantrone are mildly toxic to mesenchymal stem cells, but no phenotypic changes or cell death have been reported. MSCs isolated from doxorubicin-treated rats showed activated DNA damage response pathways, S-phase arrest, and increased sub$G_1$ subpopulation, whereas mitoxantrone caused premature senescence in MSCs from dental pulp and dermal fibroblasts, suggesting that topoisomerase II inhibition also severely damages MSCs (82, 83). Importantly, this work did not compare the sensitivity of MSCs to cancer cells.

TPEN is a cell permeable $Zn^{2+}$ chelator that is used to induce oxidative stress through dysregulation of ROS detoxification (84, 85). The sensitivity of MSCs to ROS remains unclear: some reports indicate that MSCs have lower basal levels of ROS and higher levels of the antioxidant glutathione, which protects cells from oxidative attacks (86), while other reports indicate that MSCs are more sensitive to ROS than differentiated cells, ROS accumulation leading to DNA damage and senescence, and that exogenous antioxidants are required to restore resistance to oxidative stress (87, 88). In our experiments, TPEN treatment was equally toxic to MSCs and cancer cells, suggesting that MSCs do not benefit from ROS-mediated damage.

The antimetabolite drug methotrexate, used to treat cancer and rheumatoid arthritis, interferes with thymidine synthesis by DHFR. The effects of methotrexate depend largely on the expression and structure of DHFR. Mutations in the active site of the enzyme or lower expression levels can render cells resistant to drugs (89). Consistent with our findings, Perez et al. reported that MSCs showed resistance to antimetabolites such as 5-fluorouracil and gemcitabine, and retained their stemness after treatment, probably due

to increased DNA metabolism and increased expression of multidrug resistance transporters (90). In our case, the only significant outlier was the A431 cell line, which was found to be highly sensitive to this compound, probably due to cell-specific DHFR status or the fact that A431 is the only p53 mutant in the cell line group (91).

Nutlin-3 is a potent inhibitor of the MDM2-p53 interaction and is designed to selectively kill wild-type p53-expressing cells (92). In our tests, only A431 was found to be resistant to nutlin-3, the only cell line with mutant p53 expression (Fig. 5.).

Analyzing DNA damage in MSCs and cancer cells after various treatments showed how differently the two cell types responded to toxic insults. In cytotoxicity assays, doxorubicin was equally toxic to MSCs and cancer cells; however, there were fewer DNA double-strand breaks (DSBs) in MSCs, indicating increased DNA repair. Although it is also known that MSCs can successfully repair DSBs after treatment with drugs, such as bleomycin, it was still not sufficient to protect cells from the cytotoxic effects of doxorubicin. In addition, nutlin-3 did not cause DNA damage only in cancer cells but killed only MSCs expressing p53-wt, suggesting that the amount of DNA DSBs does not correctly predict survival after drug treatment (Fig. 8.).

Treatment-induced ROS generation was also examined, but surprisingly, only nutlin-3 significantly increased ROS levels in cancer cells and MSCs. Although others have hypothesized that nutlin-3 induces ROS by increasing p53 and mitochondrial translocation levels, leading to increased ROS, in our assay, both $p53^{+/+}$ cells (MSCs) and $p53^{-/-}$ (A431) showed strong increase, but again only MSCs were killed after treatment (Fig. 8.).

The most notable outcome was that MSCs are unable to die via apoptosis. Other research studies suggest that MSCs have a higher threshold for apoptosis (77), but the exact magnitude of this phenomenon has never been demonstrated before. Some annexin-positive, late apoptotic cells were observed in the cultures of MSCs after treatment with high concentrations of doxorubicin and nutlin-3 (1μM and 50μM, respectively); however, no distinct, apoptotic populations were observed and when the gating strategy was different, these cells were lost at the late stage of apoptosis, indicating that treatment caused an extremely high level of apoptosis in cancer cells that did not activate the same cell death pathways in MSCs. However, the same concentration of doxorubicin and

nutlin-3, but not cisplatin, led to necrotic cell death in MSCs, suggesting that mesenchymal stem cells are susceptible to death by chemotherapy, but the mechanism is different. We failed to induce apoptosis in MSCs using multiple concentrations of mitoxantrone, staurosporine (a multiple kinase inhibitor), $H_2O_2$ (oxidative stress inducer) and $CoCl_2$ (hypoxia inducer). Others have reported that chemotherapy can induce apoptosis in MSCs; however, these investigations have shown only a minor increase in cleaved caspase-3 or annexin-V binding (76, 83, 90, 93). This observation suggests that MSCs are inherently unable to die by apoptosis or prefer other modes of cell death (Fig. 9.).

To assess the extent to which MSCs transition into senescence instead of death, the function of the SA-ß-GAL was studied after 12 days of treatment with the drugs, but no significant differences were found. The only change observed was a decrease in the proliferation rate in both cell types. As cancer cells have been shown to die following drug treatment, one possible explanation is that MSCs reduce the rate of their cell cycle progression and take time to avoid apoptosis, and follow a different path instead.

Overall, our results demonstrate significant differences in the response of MSCs and cancer cells to drugs, suggesting that the complex nature of the TME is likely to have a significant impact on cancer treatment. These findings will facilitate the design of rational combinations of drugs that target both mesenchymal stem cells and cancer cells in the tumor microenvironment.

To establish our co-culture system of MSCs and cancer cells, we first analyzed the effects of 2D co-culturing on cytokine secretion. Although growing the two cell types together did not induce the secretion of different cytokines compared to mono-cultures, the secretion profile of the already detected molecules was changed (Fig. 11.). For example, the concentration of CCL5 was reduced in co-cultures despite being secreted by A431 cells. As CCL5 is an inflammatory cytokine, which increases tumor growth, induces extracellular matrix remodeling and enhances tumor cell migration (94), its decrease can be explained by the remarkable anti-inflammatory effect of MSCs (95), suggesting that tumor-naive MSCs can slow down cancer progression by altering the inflammatory TME. Interestingly, the IL6-IL8 axis shifted in co-cultures: while IL-8 was secreted by both cells in mono-cultures, its level decreased in co-cultures, but, simultaneously, the

concentration of IL-6 increased despite the fact that MSCs secreted only low amount of it and A431 secrete none. These changes suggest that only a short-term co-culturing could alter the behaviour of both cell types.

This effect could also explain how MSCs promote cancer cell growth and survival at certain Ad-MSC:A431 ratios (Fig. 13.). There are serious discrepancies around the initial role of MSCs in early tumor development, with some studies claiming that MSCs actively suppress cancer cells, while other works show the opposite. For example, the viability of MDA-MB-231 breast cancer cells was reduced after co-cultured with MSCs due to the inhibition of notch signaling, an essential pathway for tumorigenesis (96) or, similarly, MSCs have been reported to inhibit the growth of breast cancer cells through disrupting the Wnt-pathway (97). In addition, MSCs could regulate AKT activity in Kaposi's sarcoma to limit tumor growth in vivo (98), increase mRNA expression of caspase 3 and p21, a negative regulator of cell cycle in tumor cells and can stop cancer from spreading both in vitro and in vivo by causing cancer cells to undergo apoptosis and $G_0/G_1$ phase arrest (52). Conversely, MSCs (99) induce angiogenesis (100), suppress immune response and immune cell infiltration at the tumor site (101), increase motility and migration (102) and promote drug resistance (103). Our results suggest that the anti- or pro-tumorigenic role of MSCs may depend on the MSC - cancer cell ratio in the TME, as we observed MSCs support cancer cell proliferation and survive only at certain proportions. Moreover, despite some growth benefit in 2D co-cultures, drug resistance did not emerge in cancer cells, which could mean that physical proximity and altered cytokine secretion profile are not sufficient to protect the cells from cytotoxic drugs (Fig. 13.).

Surprisingly, the established 3D co-cultures were organized around the same pattern: MSCs provide a dense interior feeder core, while the A431 cells form a mantle-like outer layer (Fig. 15.). It is not fully understood whether this structure is specific to these two cell lines or not; however we have found reports with quite similar 3D composition of human lung cancer cells and adipose-tissue derived from mouse MSCs, using a thin chitosan-hyaluronan matrix-based substratum, called the “core-shell structure” (104). On the other hand, in a thought-provoking work on how cancer cells cannibalize MSCs and enter dormancy, the results suggest that this happens the other way around: MSCs

virtually encapsulate cancer cells in 3D spheroids (105). This discrepancy may arise from the cancer cell lines selected. Similarly to Han et al., we used cell lines with epithelial phenotype (A431 and A549), while the study by Bartosh et al., on MDA-MB-231 contained a well-known post-EMT cell line with mesenchymal morphology. This may explain the differences in the inner structures of the established spheroids.

Our study identified a novel but rare subpopulation of cells that had fluorescent properties of both Ad-MSC-GFP-3 and A431-mCh (Fig. 16.). Fluorescent microscopy revealed that these cells showed a larger size compared to cancer cells and different morphology compared to MSCs, but most importantly, these cells had multiple nuclei. This phenomenon was previously described by Liu et al. when squamous cell carcinoma (SCC) cells were co-cultured with bone marrow MSCs (74). Similar to our findings, these double fluorescent cells were rare (~1.6%), had altered morphology and synthesized stress fibers, although only mesenchymal morphology was observed in this subpopulation, Liu et al. found mainly epithelial morphology in the double fluorescent population, which they termed MSC/SCC fused cells. In addition, they claim that these cells are cancer cells that have somehow fused with MSC and have even shown tumorigenic potential. In our hands, the double fluorescent cells are more likely to be MSCs with incorporated cancer cells, but their true origin and role in progression and drug resistance have not been studied.

The most intriguing observations were made during the study of 3D spheroids. A431 spheroids could not grow under any conditions when cultured alone; however, even the smallest number of additional MSCs was sufficient, not only to stabilize cell number and avoid shrinking, but also to support some growth (Fig. 15.). In addition, co-culture with MSCs increased drug tolerability of A431 cells, and although even 2μM cisplatin inhibited proliferation and killed cells in 2D, treatment with 10μM cisplatin was tolerated in 3D co-cultures. This result is even more significant if we consider that cancer cells are located in the outer layer (in the “shell”) of the spheroid and are not physically protected by the MSCs. Surprisingly, when we targeted the MSCs with nutlin-3, despite the diminishing inner core and the dying cells, the effect of the MSCs was still sufficient to support A431 cells. There are a number of known ways in which MSCs promote drug resistance in cancer cells, mainly through the secretion of cytokines such as IL-6, IL-7

and IL-8, for example in head and neck carcinomas where these molecules induce paclitaxel resistance (106). In our system, the overexpression of IL-6 and IL-8 was not sufficient to increase drug resistance in cancer cells, suggesting that either another factor or a physical interaction between cell types is missing.

In a recently published work, the relationship between the quantity of the stromal compartment and prognosis was thoroughly analyzed across 16 solid tumor types (107). The results challenged the common view that a more reactive stroma in tumors correlates with a poorer prognosis. Our findings support this argument and show that different levels of ratio, physical proximity, and secreted cytokines are required for MSCs to help cancer cells survive. In summary, our work suggests that MSCs may play a role in cancer drug resistance, but this effect may depend on other circumstances that have to be accounted for.

## 6. Conclusions

➤ As expected, MSCs show increased tolerance to certain compounds, but surprisingly, these cells were found to be more sensitive or similarly sensitive to other compounds than tumor cells. This effect cannot be explained by differences in proliferation rate.

➤ Despite the fact that the treatments applied were designed to induce apoptosis, MSCs showed no signs of programmed cell death, suggesting that these cells prefer other pathways or mechanisms.

➤ Treatment-induced DNA damage and ROS induction are likely to play a role in determining cell fate, but their presence is not sufficient to predict the outcome, as neither correlated with drug response. They do not explain treatment-induced senescence (TIS) of MSCs, as no signs of TIS were observed.

➤ MSCs and cancer cells co-cultured in 3D spheroids are organized in a surprising outer shell (cancer cells) - inner core (MSCs) structure.

➤ Co-culturing MSCs and cancer cells for 5 days slightly changes cytokine secretion. Although it is not sufficient to trigger the secretion of novel chemokines and cytokines, it may change the levels of the originally secreted ones. 2D co-culturing of MSCs and cancer cells has no effect on cancer cell survival and drug sensitivity, but 3D spheroids in the presence of internal MSCs rescued cancer cells and significantly increased drug tolerability.

➤ Analyzing the co-cultures with flow cytometry revealed a new $GFP^+/mCh^+$ cell population showing positivity to both fluorescent tags. These double positive ‘hybrid’ cells show MSC-like morphology, which may suggest that MSCs may ‘cannibalize’ cancer cells.

## 7. Summary

Targeting the TME has shown promising results in both preclinical and clinical studies as a therapeutic strategy for various types of cancer. Disrupting the stromal-cancer cell interactions can inhibit tumor growth, reduce metastatic spread, and improve patient outcomes.

As tumor microenvironment plays a pivotal role in tumor development, our work sheds light on how MSCs and cancer cells respond to various types of chemotherapeutics in 2D and 3D, as well as in co-cultures. Combating drug resistance is one of the greatest challenges in cancer treatment and despite the fact that tumor microenvironment may be an integral part of therapy failure, we still do not fully understand the role of MSCs in it. We have selected nine chemotherapeutic agents with different mechanisms of action, tested them on MSCs and cancer cells, and showed for the first time that MSCs are also susceptible to certain drugs, no matter whether their proliferation rate is significantly lower compared to cancer cells. Strikingly, no signs of apoptosis were observed in MSCs, suggesting alternative mechanisms of cell death.

We also created a novel and reproducible 3D spheroid model to study the interactions of MSCs and cancer cells in a 3D environment. Using this model, we demonstrated that close physical proximity of MSCs is required to support cancer cell survival during chemotherapeutic treatment, as no increased cancer cell drug tolerance was found in 2D co-cultures.

The TME is a complex system that plays a major role in tumor development and treatment response. Understanding its true role could change the game, opening new avenues for designing smart drugs to target MSCs alone or in combination with cancer cells to enhance therapeutic efficacy. From a practical point of view, our results can be used as a template for in vitro ascertainment of patient-derived tumors, using not only the cancer cells but also CA-MSCs to construct spheroids that more accurately model drug response.

It is impossible to predict what TME research holds for the future, but it will certainly be exciting and important. We hope that the observations we have made and the models we have developed can contribute to new discoveries in the field.

## 8. References


1. Sung H, Ferlay J, Siegel RL, Laversanne M, Soerjomataram I, Jemal A, et al. Global Cancer Statistics 2020: GLOBOCAN Estimates of Incidence and Mortality Worldwide for 36 Cancers in 185 Countries. CA Cancer J Clin. 2021;71(3):209-49.
2. Windt T, Toth S, Patik I, Sessler J, Kucsma N, Szepesi A, et al. Identification of anticancer OATP2B1 substrates by an in vitro triple-fluorescence-based cytotoxicity screen. Arch Toxicol. 2019;93(4):953-64.
3. Hajdu SI. 2000 years of chemotherapy of tumors. Cancer. 2005;103(6):1097-102.
4. Sun X, Zhao P, Lin J, Chen K, Shen J. Recent advances in access to overcome cancer drug resistance by nanocarrier drug delivery system. Cancer Drug Resist. 2023;6(2):390-415.
5. Roberti A, Valdes AF, Torrecillas R, Fraga MF, Fernandez AF. Epigenetics in cancer therapy and nanomedicine. Clin Epigenetics. 2019;11(1):81.
6. Christie EL, Pattnaik S, Beach J, Copeland A, Rashoo N, Fereday S, et al. Multiple ABCB1 transcriptional fusions in drug resistant high-grade serous ovarian and breast cancer. Nat Commun. 2019;10(1):1295.
7. Noll EM, Eisen C, Stenzinger A, Espinet E, Muckenhuber A, Klein C, et al. CYP3A5 mediates basal and acquired therapy resistance in different subtypes of pancreatic ductal adenocarcinoma. Nat Med. 2016;22(3):278-87.
8. Helleday T, Petermann E, Lundin C, Hodgson B, Sharma RA. DNA repair pathways as targets for cancer therapy. Nat Rev Cancer. 2008;8(3):193-204.
9. Kuroda J, Puthalakath H, Cragg MS, Kelly PN, Bouillet P, Huang DC, et al. Bim and Bad mediate imatinib-induced killing of Bcr/Abl+ leukemic cells, and resistance due to their loss is overcome by a BH3 mimetic. Proc Natl Acad Sci U S A. 2006;103(40):14907-12.
10. Sugimoto Y, Tsukahara S, Oh-hara T, Isoe T, Tsuruo T. Decreased expression of DNA topoisomerase I in camptothecin-resistant tumor cell lines as determined by a monoclonal antibody. Cancer Res. 1990;50(21):6925-30.
11. Shah MA, Schwartz GK. Cell cycle-mediated drug resistance: an emerging concept in cancer therapy. Clin Cancer Res. 2001;7(8):2168-81.

12. Sun Y, Campisi J, Higano C, Beer TM, Porter P, Coleman I, et al. Treatment-induced damage to the tumor microenvironment promotes prostate cancer therapy resistance through WNT16B. Nat Med. 2012;18(9):1359-68.
13. Sharma SV, Lee DY, Li B, Quinlan MP, Takahashi F, Maheswaran S, et al. A chromatin-mediated reversible drug-tolerant state in cancer cell subpopulations. Cell. 2010;141(1):69-80.
14. Dagogo-Jack I, Shaw AT. Tumour heterogeneity and resistance to cancer therapies. Nat Rev Clin Oncol. 2018;15(2):81-94.
15. Kim SK, Cho SW. The Evasion Mechanisms of Cancer Immunity and Drug Intervention in the Tumor Microenvironment. Front Pharmacol. 2022;13:868695.
16. Vajda F, Bajtai E, Gombos B, Karai E, Hamori L, Szakacs G, et al. [Development of novel treatment strategies for drug resistant cancer]. Magy Onkol. 2021;65(2):176-87.
17. Szakacs G, Paterson JK, Ludwig JA, Booth-Genthe C, Gottesman MM. Targeting multidrug resistance in cancer. Nat Rev Drug Discov. 2006;5(3):219-34.
18. Rittierodt M, Harada K. Repetitive doxorubicin treatment of glioblastoma enhances the PGP expression--a special role for endothelial cells. Exp Toxicol Pathol. 2003;55(1):39-44.
19. Ingelman-Sundberg M, Lauschke VM. Can CYP Inhibition Overcome Chemotherapy Resistance? Trends Pharmacol Sci. 2020;41(8):503-6.
20. Wang F, Zhang X, Wang Y, Chen Y, Lu H, Meng X, et al. Activation/Inactivation of Anticancer Drugs by CYP3A4: Influencing Factors for Personalized Cancer Therapy. Drug Metab Dispos. 2023;51(5):543-59.
21. Baran Y, Ural AU, Gunduz U. Mechanisms of cellular resistance to imatinib in human chronic myeloid leukemia cells. Hematology. 2007;12(6):497-503.
22. Zhu X, Tian T, Ruan M, Rao J, Yang W, Cai X, et al. Expression of DNA Damage Response Proteins and Associations with Clinicopathologic Characteristics in Chinese Familial Breast Cancer Patients with BRCA1/2 Mutations. J Breast Cancer. 2018;21(3):297-305.
23. Ganapathi RN, Ganapathi MK. Mechanisms regulating resistance to inhibitors of topoisomerase II. Front Pharmacol. 2013;4:89.

24. Skubnik J, Pavlickova V, Ruml T, Rimpelova S. Current Perspectives on Taxanes: Focus on Their Bioactivity, Delivery and Combination Therapy. Plants (Basel). 2021;10(3).

25. Amjad MT, Chidharla A, Kasi A. Cancer Chemotherapy. StatPearls. Treasure Island (FL) ineligible companies. Disclosure: Anusha Chidharla declares no relevant financial relationships with ineligible companies. Disclosure: Anup Kasi declares no relevant financial relationships with ineligible companies.2024.

26. Zhuang Y, Liu K, He Q, Gu X, Jiang C, Wu J. Hypoxia signaling in cancer: Implications for therapeutic interventions. MedComm (2020). 2023;4(1):e203.

27. Teleanu RI, Chircov C, Grumezescu AM, Teleanu DM. Tumor Angiogenesis and Anti-Angiogenic Strategies for Cancer Treatment. J Clin Med. 2019;9(1).

28. Itatani Y, Kawada K, Yamamoto T, Sakai Y. Resistance to Anti-Angiogenic Therapy in Cancer-Alterations to Anti-VEGF Pathway. Int J Mol Sci. 2018;19(4).

29. Adams GP, Weiner LM. Monoclonal antibody therapy of cancer. Nat Biotechnol. 2005;23(9):1147-57.

30. Raddassi K, Berthon B, Petit JF, Lemaire G. Role of calcium in the activation of mouse peritoneal macrophages: induction of NO synthase by calcium ionophores and thapsigargin. Cell Immunol. 1994;153(2):443-55.

31. Ellebrecht CT, Bhoj VG, Nace A, Choi EJ, Mao X, Cho MJ, et al. Reengineering chimeric antigen receptor T cells for targeted therapy of autoimmune disease. Science. 2016;353(6295):179-84.

32. Denkert C, Loibl S, Noske A, Roller M, Muller BM, Komor M, et al. Tumor-associated lymphocytes as an independent predictor of response to neoadjuvant chemotherapy in breast cancer. J Clin Oncol. 2010;28(1):105-13.

33. Zhang X, Lin Y, Gillies RJ. Tumor pH and its measurement. J Nucl Med. 2010;51(8):1167-70.

34. Kato Y, Ozawa S, Miyamoto C, Maehata Y, Suzuki A, Maeda T, et al. Acidic extracellular microenvironment and cancer. Cancer Cell Int. 2013;13(1):89.

35. Emami Nejad A, Najafgholian S, Rostami A, Sistani A, Shojaeifar S, Esparvarinha M, et al. The role of hypoxia in the tumor microenvironment and development of cancer stem cell: a novel approach to developing treatment. Cancer Cell Int. 2021;21(1):62.

36. Lemus-Varela ML, Flores-Soto ME, Cervantes-Munguia R, Torres-Mendoza BM, Gudino-Cabrera G, Chaparro-Huerta V, et al. Expression of HIF-1 alpha, VEGF and EPO in peripheral blood from patients with two cardiac abnormalities associated with hypoxia. Clin Biochem. 2010;43(3):234-9.

37. Lum JJ, Bui T, Gruber M, Gordan JD, DeBerardinis RJ, Covello KL, et al. The transcription factor HIF-1alpha plays a critical role in the growth factor-dependent regulation of both aerobic and anaerobic glycolysis. Genes Dev. 2007;21(9):1037-49.

38. Rashid ZA, Bardaweel SK. Novel Matrix Metalloproteinase-9 (MMP-9) Inhibitors in Cancer Treatment. Int J Mol Sci. 2023;24(15).

39. D'Souza N, Burns JS, Grisendi G, Candini O, Veronesi E, Piccinno S, et al. MSC and Tumors: Homing, Differentiation, and Secretion Influence Therapeutic Potential. Adv Biochem Eng Biotechnol. 2013;130:209-66.

40. Garnier D, Ratcliffe E, Briand J, Cartron PF, Oliver L, Vallette FM. The Activation of Mesenchymal Stem Cells by Glioblastoma Microvesicles Alters Their Exosomal Secretion of miR-100-5p, miR-9-5p and let-7d-5p. Biomedicines. 2022;10(1).

41. Liang W, Chen X, Zhang S, Fang J, Chen M, Xu Y, et al. Mesenchymal stem cells as a double-edged sword in tumor growth: focusing on MSC-derived cytokines. Cell Mol Biol Lett. 2021;26(1):3.

42. Xia B, Tian C, Guo S, Zhang L, Zhao D, Qu F, et al. c-Myc plays part in drug resistance mediated by bone marrow stromal cells in acute myeloid leukemia. Leuk Res. 2015;39(1):92-9.

43. Wang W, Zhong W, Yuan J, Yan C, Hu S, Tong Y, et al. Involvement of Wnt/beta-catenin signaling in the mesenchymal stem cells promote metastatic growth and chemoresistance of cholangiocarcinoma. Oncotarget. 2015;6(39):42276-89.

44. E OR, Dhami SPS, Baev DV, Ortutay C, Halpin-McCormick A, Morrell R, et al. Repression of Mcl-1 expression by the CDC7/CDK9 inhibitor PHA-767491 overcomes bone marrow stroma-mediated drug resistance in AML. Sci Rep. 2018;8(1):15752.

45. Akimoto K, Kimura K, Nagano M, Takano S, To'a Salazar G, Yamashita T, et al. Umbilical cord blood-derived mesenchymal stem cells inhibit, but adipose tissue-derived mesenchymal stem cells promote, glioblastoma multiforme proliferation. Stem Cells Dev. 2013;22(9):1370-86.

46. Liu ZW, Zhang YM, Zhang LY, Zhou T, Li YY, Zhou GC, et al. Duality of Interactions Between TGF-beta and TNF-alpha During Tumor Formation. Front Immunol. 2021;12:810286.

47. Rahmatizadeh F, Gholizadeh-Ghaleh Aziz S, Khodadadi K, Lale Ataei M, Ebrahimie E, Soleimani Rad J, et al. Bidirectional and Opposite Effects of Naive Mesenchymal Stem Cells on Tumor Growth and Progression. Adv Pharm Bull. 2019;9(4):539-58.

48. Chen Q, Shou P, Zheng C, Jiang M, Cao G, Yang Q, et al. Fate decision of mesenchymal stem cells: adipocytes or osteoblasts? Cell Death Differ. 2016;23(7):1128-39.

49. Xuan X, Tian C, Zhao M, Sun Y, Huang C. Mesenchymal stem cells in cancer progression and anticancer therapeutic resistance. Cancer Cell Int. 2021;21(1):595.

50. Norozi F, Ahmadzadeh A, Shahrabi S, Vosoughi T, Saki N. Mesenchymal stem cells as a double-edged sword in suppression or progression of solid tumor cells. Tumour Biol. 2016;37(9):11679-89.

51. Ramasamy R, Lam EW, Soeiro I, Tisato V, Bonnet D, Dazzi F. Mesenchymal stem cells inhibit proliferation and apoptosis of tumor cells: impact on in vivo tumor growth. Leukemia. 2007;21(2):304-10.

52. Lu YR, Yuan Y, Wang XJ, Wei LL, Chen YN, Cong C, et al. The growth inhibitory effect of mesenchymal stem cells on tumor cells in vitro and in vivo. Cancer Biol Ther. 2008;7(2):245-51.

53. Wang Y, Liu J, Ma X, Cui C, Deenik PR, Henderson PKP, et al. Real-time imaging of senescence in tumors with DNA damage. Sci Rep. 2019;9(1):2102.

54. Zhang HR, Wang XD, Yang X, Chen D, Hao J, Cao R, et al. An FGFR inhibitor converts the tumor promoting effect of TGF-beta by the induction of fibroblast-associated genes of hepatoma cells. Oncogene. 2017;36(27):3831-41.

55. Luraghi P, Reato G, Cipriano E, Sassi F, Orzan F, Bigatto V, et al. MET signaling in colon cancer stem-like cells blunts the therapeutic response to EGFR inhibitors. Cancer Res. 2014;74(6):1857-69.

56. Zhang D, Li L, Jiang H, Li Q, Wang-Gillam A, Yu J, et al. Tumor-Stroma IL1beta-IRAK4 Feedforward Circuitry Drives Tumor Fibrosis, Chemoresistance, and Poor Prognosis in Pancreatic Cancer. Cancer Res. 2018;78(7):1700-12.

57. Jia C, Wang G, Wang T, Fu B, Zhang Y, Huang L, et al. Cancer-associated Fibroblasts induce epithelial-mesenchymal transition via the Transglutaminase 2-dependent IL-6/IL6R/STAT3 axis in Hepatocellular Carcinoma. Int J Biol Sci. 2020;16(14):2542-58.

58. Nurmik M, Ullmann P, Rodriguez F, Haan S, Letellier E. In search of definitions: Cancer-associated fibroblasts and their markers. Int J Cancer. 2020;146(4):895-905.

59. Louault K, Bonneaud TL, Seveno C, Gomez-Bougie P, Nguyen F, Gautier F, et al. Interactions between cancer-associated fibroblasts and tumor cells promote MCL-1 dependency in estrogen receptor-positive breast cancers. Oncogene. 2019;38(17):3261-73.

60. Kong HJ, Kwon EJ, Kwon OS, Lee H, Choi JY, Kim YJ, et al. Crosstalk between YAP and TGFbeta regulates SERPINE1 expression in mesenchymal lung cancer cells. Int J Oncol. 2021;58(1):111-21.

61. Seker F, Cingoz A, Sur-Erdem I, Erguder N, Erkent A, Uyulur F, et al. Identification of SERPINE1 as a Regulator of Glioblastoma Cell Dispersal with Transcriptome Profiling. Cancers (Basel). 2019;11(11).

62. Whelan DS, Caplice NM, Clover AJP. Mesenchymal stromal cell derived CCL2 is required for accelerated wound healing. Sci Rep. 2020;10(1):2642.

63. Lee S, Kim OJ, Lee KO, Jung H, Oh SH, Kim NK. Enhancing the Therapeutic Potential of CCL2-Overexpressing Mesenchymal Stem Cells in Acute Stroke. Int J Mol Sci. 2020;21(20).

64. Swamydas M, Ricci K, Rego SL, Dreau D. Mesenchymal stem cell-derived CCL-9 and CCL-5 promote mammary tumor cell invasion and the activation of matrix metalloproteinases. Cell Adh Migr. 2013;7(3):315-24.

65. Dorronsoro A, Lang V, Ferrin I, Fernandez-Rueda J, Zabaleta L, Perez-Ruiz E, et al. Intracellular role of IL-6 in mesenchymal stromal cell immunosuppression and proliferation. Sci Rep. 2020;10(1):21853.

66. Tanaka T, Narazaki M, Masuda K, Kishimoto T. Regulation of IL-6 in Immunity and Diseases. Adv Exp Med Biol. 2016;941:79-88.

67. Wang L, Li Y, Zhang X, Liu N, Shen S, Sun S, et al. Paracrine interleukin-8 affects mesenchymal stem cells through the Akt pathway and enhances human umbilical vein endothelial cell proliferation and migration. Biosci Rep. 2021;41(5).

68. Wang Y, Liu J, Jiang Q, Deng J, Xu F, Chen X, et al. Human Adipose-Derived Mesenchymal Stem Cell-Secreted CXCL1 and CXCL8 Facilitate Breast Tumor Growth By Promoting Angiogenesis. Stem Cells. 2017;35(9):2060-70.
69. Radfar P, Ding L, de la Fuente LR, Aboulkheyr H, Gallego-Ortega D, Warkiani ME. Rapid metabolomic screening of cancer cells via high-throughput static droplet microfluidics. Biosens Bioelectron. 2023;223:114966.
70. Kumar A, Taghi Khani A, Sanchez Ortiz A, Swaminathan S. GM-CSF: A Double-Edged Sword in Cancer Immunotherapy. Front Immunol. 2022;13:901277.
71. Kim J, Kim NK, Park SR, Choi BH. GM-CSF Enhances Mobilization of Bone Marrow Mesenchymal Stem Cells via a CXCR4-Medicated Mechanism. Tissue Eng Regen Med. 2019;16(1):59-68.
72. Tang B, Li X, Liu Y, Chen X, Li X, Chu Y, et al. The Therapeutic Effect of ICAM-1-Overexpressing Mesenchymal Stem Cells on Acute Graft-Versus-Host Disease. Cell Physiol Biochem. 2018;46(6):2624-35.
73. Li X, Wang Q, Ding L, Wang YX, Zhao ZD, Mao N, et al. Intercellular adhesion molecule-1 enhances the therapeutic effects of MSCs in a dextran sulfate sodium-induced colitis models by promoting MSCs homing to murine colons and spleens. Stem Cell Res Ther. 2019;10(1):267.
74. Liu C, Billet S, Choudhury D, Cheng R, Haldar S, Fernandez A, et al. Bone marrow mesenchymal stem cells interact with head and neck squamous cell carcinoma cells to promote cancer progression and drug resistance. Neoplasia. 2021;23(1):118-28.
75. Plava J, Burikova M, Cihova M, Trnkova L, Smolkova B, Babal P, et al. Chemotherapy-triggered changes in stromal compartment drive tumor invasiveness and progression of breast cancer. J Exp Clin Cancer Res. 2021;40(1):302.
76. Nicolay NH, Ruhle A, Perez RL, Trinh T, Sisombath S, Weber KJ, et al. Mesenchymal stem cells exhibit resistance to topoisomerase inhibition. Cancer Lett. 2016;374(1):75-84.
77. Mueller LP, Luetzkendorf J, Mueller T, Reichelt K, Simon H, Schmoll HJ. Presence of mesenchymal stem cells in human bone marrow after exposure to chemotherapy: evidence of resistance to apoptosis induction. Stem Cells. 2006;24(12):2753-65.

78. Liang W, Xia H, Li J, Zhao RC. Human adipose tissue derived mesenchymal stem cells are resistant to several chemotherapeutic agents. Cytotechnology. 2011;63(5):523-30.

79. Baguley BC, Marshall ES, Whittaker JR, Dotchin MC, Nixon J, McCrystal MR, et al. Resistance mechanisms determining the in vitro sensitivity to paclitaxel of tumour cells cultured from patients with ovarian cancer. Eur J Cancer. 1995;31A(2):230-7.

80. Gascoigne KE, Taylor SS. Cancer cells display profound intra- and interline variation following prolonged exposure to antimitotic drugs. Cancer Cell. 2008;14(2):111-22.

81. Schmidt-Hieber M, Busse A, Reufi B, Knauf W, Thiel E, Blau IW. Bendamustine, but not fludarabine, exhibits a low stem cell toxicity in vitro. J Cancer Res Clin Oncol. 2009;135(2):227-34.

82. Oliveira MS, Carvalho JL, Campos AC, Gomes DA, de Goes AM, Melo MM. Doxorubicin has in vivo toxicological effects on ex vivo cultured mesenchymal stem cells. Toxicol Lett. 2014;224(3):380-6.

83. Seifrtova M, Havelek R, Soukup T, Filipova A, Mokry J, Rezacova M. Mitoxantrone ability to induce premature senescence in human dental pulp stem cells and human dermal fibroblasts. J Physiol Pharmacol. 2013;64(2):255-66.

84. Hashemi M, Ghavami S, Eshraghi M, Booy EP, Los M. Cytotoxic effects of intra and extracellular zinc chelation on human breast cancer cells. Eur J Pharmacol. 2007;557(1):9-19.

85. Mendivil-Perez M, Velez-Pardo C, Jimenez-Del-Rio M. TPEN induces apoptosis independently of zinc chelator activity in a model of acute lymphoblastic leukemia and ex vivo acute leukemia cells through oxidative stress and mitochondria caspase-3- and AIF-dependent pathways. Oxid Med Cell Longev. 2012;2012:313275.

86. Valle-Prieto A, Conget PA. Human mesenchymal stem cells efficiently manage oxidative stress. Stem Cells Dev. 2010;19(12):1885-93.

87. Orciani M, Gorbi S, Benedetti M, Di Benedetto G, Mattioli-Belmonte M, Regoli F, et al. Oxidative stress defense in human-skin-derived mesenchymal stem cells versus human keratinocytes: Different mechanisms of protection and cell selection. Free Radic Biol Med. 2010;49(5):830-8.

88. Ko E, Lee KY, Hwang DS. Human umbilical cord blood-derived mesenchymal stem cells undergo cellular senescence in response to oxidative stress. Stem Cells Dev. 2012;21(11):1877-86.

89. Volpato JP, Fossati E, Pelletier JN. Increasing methotrexate resistance by combination of active-site mutations in human dihydrofolate reductase. J Mol Biol. 2007;373(3):599-611.

90. Lopez Perez R, Munz F, Vidoni D, Ruhle A, Trinh T, Sisombath S, et al. Mesenchymal stem cells preserve their stem cell traits after exposure to antimetabolite chemotherapy. Stem Cell Res. 2019;40:101536.

91. Reiss M, Brash DE, Munoz-Antonia T, Simon JA, Ziegler A, Vellucci VF, et al. Status of the p53 tumor suppressor gene in human squamous carcinoma cell lines. Oncol Res. 1992;4(8-9):349-57.

92. Vassilev LT, Vu BT, Graves B, Carvajal D, Podlaski F, Filipovic Z, et al. In vivo activation of the p53 pathway by small-molecule antagonists of MDM2. Science. 2004;303(5659):844-8.

93. Cruet-Hennequart S, Prendergast AM, Shaw G, Barry FP, Carty MP. Doxorubicin induces the DNA damage response in cultured human mesenchymal stem cells. Int J Hematol. 2012;96(5):649-56.

94. Aldinucci D, Borghese C, Casagrande N. The CCL5/CCR5 Axis in Cancer Progression. Cancers (Basel). 2020;12(7).

95. Regmi S, Pathak S, Kim JO, Yong CS, Jeong JH. Mesenchymal stem cell therapy for the treatment of inflammatory diseases: Challenges, opportunities, and future perspectives. Eur J Cell Biol. 2019;98(5-8):151041.

96. Mandel K, Yang Y, Schambach A, Glage S, Otte A, Hass R. Mesenchymal stem cells directly interact with breast cancer cells and promote tumor cell growth in vitro and in vivo. Stem Cells Dev. 2013;22(23):3114-27.

97. Qiao L, Xu ZL, Zhao TJ, Ye LH, Zhang XD. Dkk-1 secreted by mesenchymal stem cells inhibits growth of breast cancer cells via depression of Wnt signalling. Cancer Lett. 2008;269(1):67-77.

98. Khakoo AY, Pati S, Anderson SA, Reid W, Elshal MF, Rovira, II, et al. Human mesenchymal stem cells exert potent antitumorigenic effects in a model of Kaposi's sarcoma. J Exp Med. 2006;203(5):1235-47.

99. Coffman LG, Pearson AT, Frisbie LG, Freeman Z, Christie E, Bowtell DD, et al. Ovarian Carcinoma-Associated Mesenchymal Stem Cells Arise from Tissue-Specific Normal Stroma. Stem Cells. 2019;37(2):257-69.
100. Spaeth EL, Dembinski JL, Sasser AK, Watson K, Klopp A, Hall B, et al. Mesenchymal stem cell transition to tumor-associated fibroblasts contributes to fibrovascular network expansion and tumor progression. PLoS One. 2009;4(4):e4992.
101. Han Z, Tian Z, Lv G, Zhang L, Jiang G, Sun K, et al. Immunosuppressive effect of bone marrow-derived mesenchymal stem cells in inflammatory microenvironment favours the growth of B16 melanoma cells. J Cell Mol Med. 2011;15(11):2343-52.
102. Halpern JL, Kilbarger A, Lynch CC. Mesenchymal stem cells promote mammary cancer cell migration in vitro via the CXCR2 receptor. Cancer Lett. 2011;308(1):91-9.
103. Coffman LG, Choi YJ, McLean K, Allen BL, di Magliano MP, Buckanovich RJ. Human carcinoma-associated mesenchymal stem cells promote ovarian cancer chemotherapy resistance via a BMP4/HH signaling loop. Oncotarget. 2016;7(6):6916-32.
104. Han HW, Hsu SH. Chitosan-hyaluronan based 3D co-culture platform for studying the crosstalk of lung cancer cells and mesenchymal stem cells. Acta Biomater. 2016;42:157-67.
105. Bartosh TJ, Ullah M, Zeitouni S, Beaver J, Prockop DJ. Cancer cells enter dormancy after cannibalizing mesenchymal stem/stromal cells (MSCs). Proc Natl Acad Sci U S A. 2016;113(42):E6447-E56.
106. Scherzed A, Hackenberg S, Froelich K, Kessler M, Koehler C, Hagen R, et al. BMSC enhance the survival of paclitaxel treated squamous cell carcinoma cells in vitro. Cancer Biol Ther. 2011;11(3):349-57.
107. Micke P, Strell C, Mattsson J, Martin-Bernabe A, Brunnstrom H, Huvila J, et al. The prognostic impact of the tumour stroma fraction: A machine learning-based analysis in 16 human solid tumour types. EBioMedicine. 2021;65:103269.

## 9. Bibliography of the candidate's publications

**PhD dissertation based on the following publications:**

Vajda F, Bajtai E, Gombos B, Karai E, Hámori L, Szakács G, Füredi A. Új stratégiák fejlesztése a gyógyszerrezisztens daganatok kezeléséhez [Development of novel treatment strategies for drug resistant cancer]. Magy Onkol. 2021 Jun 3;65(2):176-187. Hungarian. Epub 2021 May 9. PMID: 34081765.

Vajda F, Szepesi Á, Várady G, Sessler J, Kiss D, Erdei Z, Szebényi K, Német K, Szakács G, Füredi A. Comparison of Different Clinical Chemotherapeutical Agents' Toxicity and Cell Response on Mesenchymal Stem Cells and Cancer Cells. Cells. 2022 Sep 20;11(19):2942. doi: 10.3390/cells11192942. PMID: 36230904; PMCID: PMC9563435.

Vajda F, Szepesi Á, Erdei Z, Szabó E, Várady G, Kiss D, Héja L, Német K, Szakács G, Füredi A. Mesenchymal Stem Cells Increase Drug Tolerance of A431 Cells Only in 3D Spheroids, Not in 2D Co-Cultures. Int J Mol Sci. 2024 Apr 20;25(8):4515. doi: 10.3390/ijms25084515. PMID: 38674102; PMCID: PMC11049889.

**Other publications:**

Ujhelly O, Szabo V, Kovacs G, Vajda F, Mallok S, Prorok J, Acsai K, Hegedus Z, Krebs S, Dinnyes A, Pirity MK. Lack of Rybp in Mouse Embryonic Stem Cells Impairs Cardiac Differentiation. Stem Cells Dev. 2015 Sep 15;24(18):2193-205. doi: 10.1089/scd.2014.0569. Epub 2015 Jun 25. PMID: 26110923.

Gouveia RM, Vajda F, Wibowo JA, Figueiredo F, Connon CJ. YAP, ΔNp63, and β-Catenin Signaling Pathways Are Involved in the Modulation of Corneal Epithelial Stem Cell Phenotype Induced by Substrate Stiffness. Cells. 2019 Apr 12;8(4):347. doi: 10.3390/cells8040347. PMID: 31013745; PMCID: PMC6523807.

**Under revision:**

Vizvari Z, Gyorfi N, Gergo M, Varga R, Jakabfi-Csepregi R, Sari T, Furedi A, Bajtai E, Vajda F, Tadic V, Odry P, Karadi Z, Toth A., Reproducibility Analysis of Self-Produced Live Cell Assays Using Novel Bioimpedance Measurement Technology, Scientific Reports, 2024

Tóth S, Szlávik M, Mandel R, Fekecs F, Tusnady G; Vajda F; Varga N; Apáti Á, Paczal A. Kotschy A, Szakacs G. Synthesis and systematic investigation of Lepidiline A and its gold(I), silver(I) and copper(I) complexes using in vitro cancer models and multipotent stem cells. ACS Omega. 2024

## 10. Acknowledgments

In this chapter, I would like to express my gratitude to those who contributed to my PhD studies and research:

András Füredi and Gergely Szakács, my supervisors, for their help and guidance in cancer research, as well as for their mentoring and continuous support throughout the research work.

My sincere thanks go to the members of the Drug Resistant Research team, Szilárd Tóth, Dániel Kiss, Eszter Bajtai, Judit Sessler, Balázs Gombos, Lilla Hámori, and Krisztina Dolniczki. Thanks to Krisztina Mohos for her laboratory support and order management.

I am grateful for all past and present members of the Creative Cells Ltd.: Katalin Német, Margit Bakki, Áron Szepesi, Anna Szigeti, Zsolt Matula and Ferenc Uher.

I am grateful to Kornélia Szebényi and Zsuzsa Erdei for their wise advice and helpfulness with stem cells.

Last but not least, Réka Laczkó-Rigó, Virág Bujdosó-Székely and Orsolya Auerné Ungvári. Their laughter, encouragement, and shared moments in the laboratory made the scientific challenges more manageable and the successes more joyful. Thank Éva Bakos for thought-provoking questions and advice.

Finally, to my family, to my mother and T. Adorján, for their everlasting support.